Molecular Therapy
Nucleic Acids
Original Article

TraFo-CRISPR: Enhanced Genome Engineering by Transient Foamy Virus Vector-Mediated Delivery of CRISPR/Cas9 Components

Fabian Lindel,[1,2] Carolin R. Dodt,[1,2] Niklas Weidner,[1,2] Monique Noll,[1,2] Fabian Bergemann,[1,2,5] Rayk Behrendt,[3] Sarah Fischer,[1,2,6] Josephine Dietrich,[4] Marc Cartellieri,[4] Martin V. Hamann,[1,2,7] and Dirk Lindemann[1,2]

[1]Institute of Virology, Medical Faculty "Carl Gustav Carus," Technische Universität Dresden, 01307 Dresden, Germany; [2]CRTD/DFG-Center for Regenerative Therapies Dresden, Technische Universität Dresden, 01307 Dresden, Germany; [3]Institute of Immunology, Technische Universität Dresden, 01307 Dresden, Germany; [4]Cellex Patient Treatment GmbH, 01307 Dresden, Germany

The adaptation of CRISPR/Cas technology for use in mammals has revolutionized genome engineering. In particular with regard to clinical application, efficient expression of Cas9 within a narrow time frame is highly desirable to minimize the accumulation of off-target editing. We developed an effective, aptamer-independent retroviral delivery system for Cas9 mRNAs that takes advantage of a unique foamy virus (FV) capability: the efficient encapsidation and transfer of non-viral RNAs. This enabled us to create a FV vector toolbox for efficient, transient delivery (TraFo) of CRISPR/Cas9 components into different target tissues. Co-delivery of Cas9 mRNA by TraFo-Cas9 vectors in combination with retroviral, integration-deficient single guide RNA (sgRNA) expression enhanced efficacy and specificity of gene-inactivation compared with CRISPR/Cas9 lentiviral vector systems. Furthermore, separate TraFo-Cas9 delivery allowed the optional inclusion of a repair matrix for efficient gene correction or tagging as well as the addition of fluorescent negative selection markers for easy identification of off-target editing or incorrect repair events. Thus, the TraFo CRISPR toolbox represents an interesting alternative technology for gene inactivation and gene editing.

INTRODUCTION

Recent developments in genome engineering have created many new possibilities for gene therapy.[1–4] In particular, the adaptation of CRISPR/Cas systems, a natural defense machinery of bacteria and archaea against invading nucleic acids, for mammalian genome engineering has had a tremendous impact on a variety of fields including biology and medicine.[5–7] The efficiency and easy handling of the programmable CRISPR/Cas9 system made it a long-awaited tool not only for basic research but also for clinical applications.

Clinical translation of genome engineering is subject to various challenges. Inevitably, the capacity to induce specific genetic modifications always harbors the risk of producing unintended and unexpected genetic alterations. To address this problem, efforts were made to "domesticate" Cas9 for higher fidelity.[8,9] Additionally, off-target gene editing is boosted by sustained or excess expression of CRISPR components.[10–14] One approach to tackle this problem is to provide Cas9 at low concentrations and within a restricted time period. Currently used transient delivery platforms developed for such a "hit and run" strategy are transfection of *in vitro* assembled Cas9-single guide RNA (sgRNA) ribonucleoprotein (RNP) or *in vitro* transcribed *Cas9* mRNAs together with sgRNAs.[11,15,16] However, the inefficient transfer of cargo into target cells often remains a limitation for most non-viral delivery platforms.

Viral platforms for delivery of programmable nucleases are mostly based on adeno-associated viruses (AAVs), adenoviruses and retroviruses.[17–20] Established integration-competent lentiviral vector (ICLV) systems, used in many of the current clinical gene therapy trials, result in chromosomal integration of the viral genome and constitutive transgene expression. Given the accumulating risks of sustained CRISPR/Cas9 expression, such ICLV systems have a limited suitability for genome engineering in a clinical setting. Great efforts were made to address this problem. All-in-one and two-lentivirus CRISPR/Cas9 delivery systems attempt to overcome this limitation by first integrating functional CRISPR/Cas9 sequences into the genome and subsequently trying to again inactivate the *Cas9* open reading frame (ORF) by co-expression of *Cas9*-targeting sgRNAs.[21,22] However, such efforts are cumbersome, dependent on sophisticated packaging conditions, and *Cas9* inactivation cannot be ensured with absolute certainty. Additionally, different modified retroviral vector systems have been described to minimize this restriction. This includes integrase-deficient lentiviral vectors (IDLV) with enzymatically inactive retroviral integrase enzyme.[20] By definition, these

Received 15 February 2019; accepted 10 October 2019;
https://doi.org/10.1016/j.omtn.2019.10.006.

[5]Deceased

[6]Present address: Institut für Biochemie I, Uniklinik Köln, 50931 Köln, Germany

[7]Present address: Heinrich Pette Institute, Leibniz Institute for Experimental Virology, 20252 Hamburg, Germany

Correspondence: Dirk Lindemann, Institute of Virology, Medical Faculty "Carl Gustav Carus," Technische Universität Dresden, 01307 Dresden, Germany.
E-mail: dirk.lindemann@tu-dresden.de

IDLVs are deficient in genomic integration of episomal viral DNA, but this is a relative rather than an absolute property as they still have some residual, low-level, non-canonical integration capacity. Alternatively, virally encapsidated Cas9 protein has been described to result in a high target specificity.[23] However, virus titers and editing efficiency are low in comparison to ICLV systems.

Foamy viruses (FVs) represent a special type of retroviruses with unique features.[24] This includes an infectious viral DNA genome, which is one of the largest among retroviruses. Furthermore, the FV envelope protein confers a very broad host cell tropism. These features in combination with the apathogenic nature of FV infections in natural and zoonotic hosts make FVs highly interesting candidates for therapeutic applications.[25,26] In the past, we and others have developed various vector systems based on FVs, which can be efficiently used to stably integrate and express foreign genetic information in a variety of different target tissues *in vitro* and *in vivo*.[27–33] Additionally, similar to IDLVs, engineered, integrase-deficient prototype FV (PFV) vectors (IDPVs) have been characterized.[34] Recently, we reported a unique PFV vector system, which enables a purely transient genetic modification of target tissues *in vitro* and *in vivo* by exploiting the special natural feature of PFV particles to encapsidate and efficiently deliver non-viral RNAs.[35,36] In this study we describe the establishment of an efficient PFV-based vector toolbox for delivery of CRISPR/Cas9 genome engineering components to different target tissues. We report here the transient PFV vector system (TraFo-Cas9) that allows for fully transient transfer and expression of *Cas9* mRNAs lacking any retroviral sequences into a wide variety of mammalian cells. When combined with integration-deficient retroviral vectors (IDRVs) enabling an episomal and largely but not completely transient sgRNA expression, efficient gene inactivation is achieved after a single exposure of target tissues. Additionally, by separating TraFo-Cas9 delivery from the IDLV or IDPV-mediated transfer of sgRNA expression cassettes, we were able to simultaneously provide repair matrices of up to 3 kb in size to induce gene editing by homology directed repair. Furthermore, optional inclusion of fluorescent reporters allowed a flow cytometric distinction of target cells with correct HDR events from those containing incorrect repair or off-target integration events.

RESULTS

Efficient Gene Inactivation by TraFo-Cas9 Delivery

Various PFV-based retroviral vector systems for efficient stable or transient genetic modification of different target tissues by *in vitro* or *in vivo* transduction have been described.[27,29–32,35] Different PFV vector supernatants were generated to compare the gene inactivation efficiency upon stable or transient delivery of genetic information encoding individual CRISPR/Cas9 editing components into U2OS-GFP target cells,[37,38] which harbor a single copy of a constitutively expressed *egfp* ORF (Figure S1).

In a two-virus vector system, *Cas9* and *egfp*-specific sgRNA encoding genetic information was packaged in separate vector particles (Figure S1). Such a vector system allowed *GFP* inactivation in up to 90% of the target cells by a single, simultaneous application of a 1:1 mixture of plain, unconcentrated virus supernatants (Figure 1A; Figure S2). The most promising two-virus combinations were particles harboring either reverse transcription-competent PFV vector genomes with integration-competent (gRNA ICPV) or integration-deficient (gRNA IDPV) sgRNA expression together with TraFo-Cas9 particles (Cas9 TraFo) fully transiently delivering *Cas9* as mRNA. Indeed, such virus combinations allowed knock out (KO) of GFP expression in 88% and 84% of the transduced U2OS-GFP cells, respectively (Figure 1A; Figure S2).

GFP inactivation assays using the two-virus vector system with 10-fold virus supernatant dilutions of Cas9 TraFo and ICPVs or IDPVs encoding *egfp*-specific sgRNAs demonstrated that sgRNA delivery is more limiting than Cas9 (Figure 1B; Figures S2A–S2D). Furthermore, *GFP* inactivation assays involving time-delayed application of the *Cas9* and *sgRNA* encoding viruses of up to 48 h revealed no major differences in gene inactivation efficiency in comparison to simultaneous transduction for most virus combinations (Figures S2E–S2H). The only exceptions were infections of cells with Cas9 TraFo particles 48 h later than with gRNA IDPV particles resulting in a significantly decreased *GFP* inactivation efficiency (Figure S2G). Additionally, in a pure TraFo approach (Figure S2H), transduction of cells with sgRNA TraFo particles 24 h after Cas9 delivery notably increased *GFP* inactivation to about 30%.

Our results indicate that a PFV-based two-virus CRIPSR/Cas9 system is perfectly able of inactivating gene expression if *Cas9* gets provided by TraFo-Cas9 particles together with ICPVs or IDPVs coding for gene-specific *sgRNAs*.

TraFo-Cas9 Vector Particle Transduction Does Not Deliver Cas9-Encoding DNA to Target Tissue

In order to get more insight into the temporal and quantitative dynamics of *Cas9*-encoding nucleic acids during TraFo-Cas9 transduction, we examined the efficiency of *Cas9* transcript encapsidation into TraFo-Cas9 vector particles (Figure 2). Therefore, we determined the amount of *Cas9* mRNA molecules associated with TraFo-Cas9 particle release by qPCR analysis. TraFo-Cas9 particle samples with simian FV *Macaca cyclopis* (SFVmcy) envelope protein (TraFo-Cas9 SE) or TraFo-Cas9 particles pseudotyped with vesicular stomatitis virus G protein (VSV-G) (TraFo-Cas9 VSV) contained $8.9 \pm 2.8 \times 10^7$ and $6.5 \pm 0.4 \times 10^7$ *Cas9* mRNA copies per mL of plain supernatant, respectively (Figure 2A). Subsequently, these TraFo-Cas9 supernatants were titrated on U2OS-GFP target cells, stably expressing a *egfp*-specific sgRNA and DsRed after ICPV transduction, and *GFP* inactivation efficiency was quantified 7 days post infection (p.i.) (Figure 2B). Incubation of U2OS-GFP sgEGFP1 cells with TraFo-Cas9 SE supernatant corresponding to 60 copies/cells (1 mL 1/30 dilution to 5×10^4 cells) resulted in a >90% *GFP* inactivation, and further dilution to 6 copies/cell (1/300) still achieved a 50% inactivation. Although *Cas9* mRNA copy numbers of TraFo-Cas9 SE supernatants were only 1.4-fold higher than those of TraFo-Cas9 VSV supernatants, their *GFP* inactivation potency on

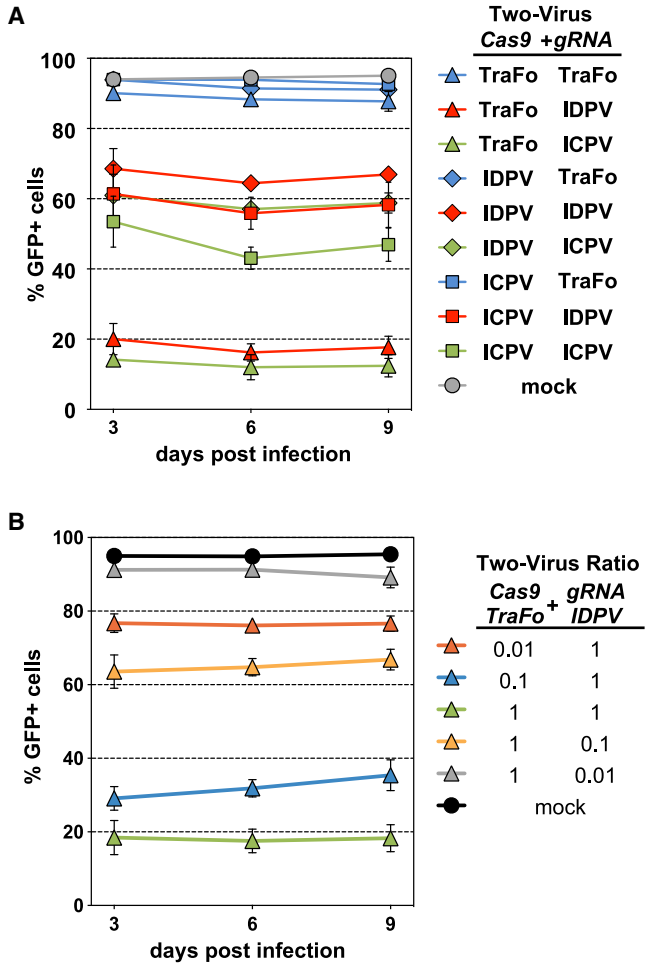

Figure 1. Efficient Gene Inactivation by Two-Virus PFV CRISPR Vector Systems by Transient TraFo-Cas9 Delivery

PFV vector particles of different composition, as indicated in the graphs' legends, were generated by transient transfection of respective expression constructs into 293T cells (see also Figure S1). *Cas9* coding sequences were transferred into target cells in terms of non-viral, RNA-polymerase-II-derived mRNA (Cas9 TraFo) or SFFV U3 promoter-driven expression cassettes embedded into integration-competent viral DNA (Cas9 ICPV) or integration-deficient DNA (Cas9 IDPV). *sgRNA* sequences were transferred into target cells in terms of RNA-polymerase-III-derived transcripts (gRNA TraFo), or U6 promoter-driven expression cassettes embedded into viral vector genomes either in form of integration-competent viral DNA (gRNA ICPV) or integration-deficient DNA (gRNA IDPV). If not mentioned otherwise, plain, cell-free 293T supernatants were used for transduction of U2OS-GFP target cells and the percentage of GFP-expressing cells was determined at different time points post infection (p.i.) as indicated. (A) *GFP* inactivation following simultaneous transduction of target cells with different, plain two-virus vector supernatant combinations as indicated at a 1:1 ratio. Means ± SD (n = 4; infections with independently produced viral supernatants) are displayed. (B) Influence of titration of TraFo-Cas9 and sgRNA IDPV vector supernatant on gene inactivation efficiency. *GFP* inactivation following simultaneous transduction of target cells with different, plain two-virus vector supernatant combinations or 10-fold serial dilutions thereof as indicated. Means ± SD (n = 4, infections with independently produced viral supernatants) are displayed.

U2OS-GFP cells was more than 10-fold higher. This suggests SE Env containing TraFo vector particles are more efficient on U2OS target cells than respective VSV-G pseudotypes.

Next we investigated the kinetics of *Cas9* RNA and DNA copy numbers in infected target cells (Figure 2C). Hence, U2OS-GFP target cells were transduced with various *Cas9*-encoding vector supernatants at different concentrations. Subsequently, cellular RNA and genomic DNA were isolated at different time points p.i. (1 day p.i. and 7 days p.i.), and the amounts of *Cas9* RNA and DNA were quantified by qPCR. Samples infected with Cas9 ICLV and IDLV particles served as a reference for stable or largely transient delivery of *Cas9*-encoding vDNA. At 1 day p.i., *Cas9*-encoding mRNA was detectable for all viral vector transduced cells in a concentration-dependent manner. In contrast, at 7 days p.i., detectable amounts of *Cas9* transcripts were only found in cells transduced with ICLV or IDLVs. Remarkably, neither early nor late after TraFo-Cas9 transduction we were able to detect any *Cas9*-encoding DNA in cells incubated with TraFo-Cas9 supernatant (Figure 2C), although the *GFP* inactivation efficiency in TraFo-Cas9 transduced samples exceeded that of Cas9 ICLV or IDLV samples at identical virus supernatant dilutions (Figure 2D). Thus TraFo-Cas9 particle preparations do not transfer *Cas9*-encoding plasmid DNA in detectable amounts into target tissue. In contrast, in cells infected with ICLV and IDLV supernatants, *Cas9*-encoding DNA was readily detectable and correlated with the concentration of vector supernatants applied (Figure 2C). In good agreement with the expected, largely episomal DNA delivery of IDLVs the amount of *Cas9*-encoding DNA in IDLV transduced cells strongly declined from 1 day p.i. to 7 days p.i. However, a certain amount of *Cas9*-encoding DNA copies (0.23 per cell at 1:30 virus dilution) remained detectable even 7 days p.i. (Figure 2C). In summary, our results demonstrate that only the TraFo-Cas9 system represents an effective and transient system at all time points examined.

Enhanced Targeting Specificity by TraFo-Cas9 Delivery in Comparison with Lentiviral Transduction

Because a shorter cellular availability of Cas9 can reduce off-target editing frequency,[11,15,16] we wanted to investigate whether the restricted time of Cas9 expression, achieved by TraFo-Cas9 delivery, effectively contributes to improved target specificity. Therefore, we made use of a recently described method to quantify the occurrence of off-target indel mutations by comparing the *GFP* inactivation efficiency of sgRNAs specific for the *egfp* ORF with 0, 1, or 2 mismatches (sgEGFPwt, m1, m2; Figures 3A–3D).[21]

First, we stably transduced U2OS-GFP target cells with ICPV sgRNA vector genomes (Figure 3A), leading to a stable co-expression of *egfp*-specific sgRNAs (sgEGFPwt, m1, m2) and DsRed (Figure 3B). Subsequently, sgRNA-expressing cell populations were incubated with dilutions of unconcentrated *Cas9*-encoding viral supernatants of ICLV or IDLV, as well as TraFo-Cas9 particles to achieve similar gene inactivation efficiencies of 74%, 58%, and 68% in DsRed and sgRNA EGFPwt-expressing cell populations at 8 days p.i., respectively

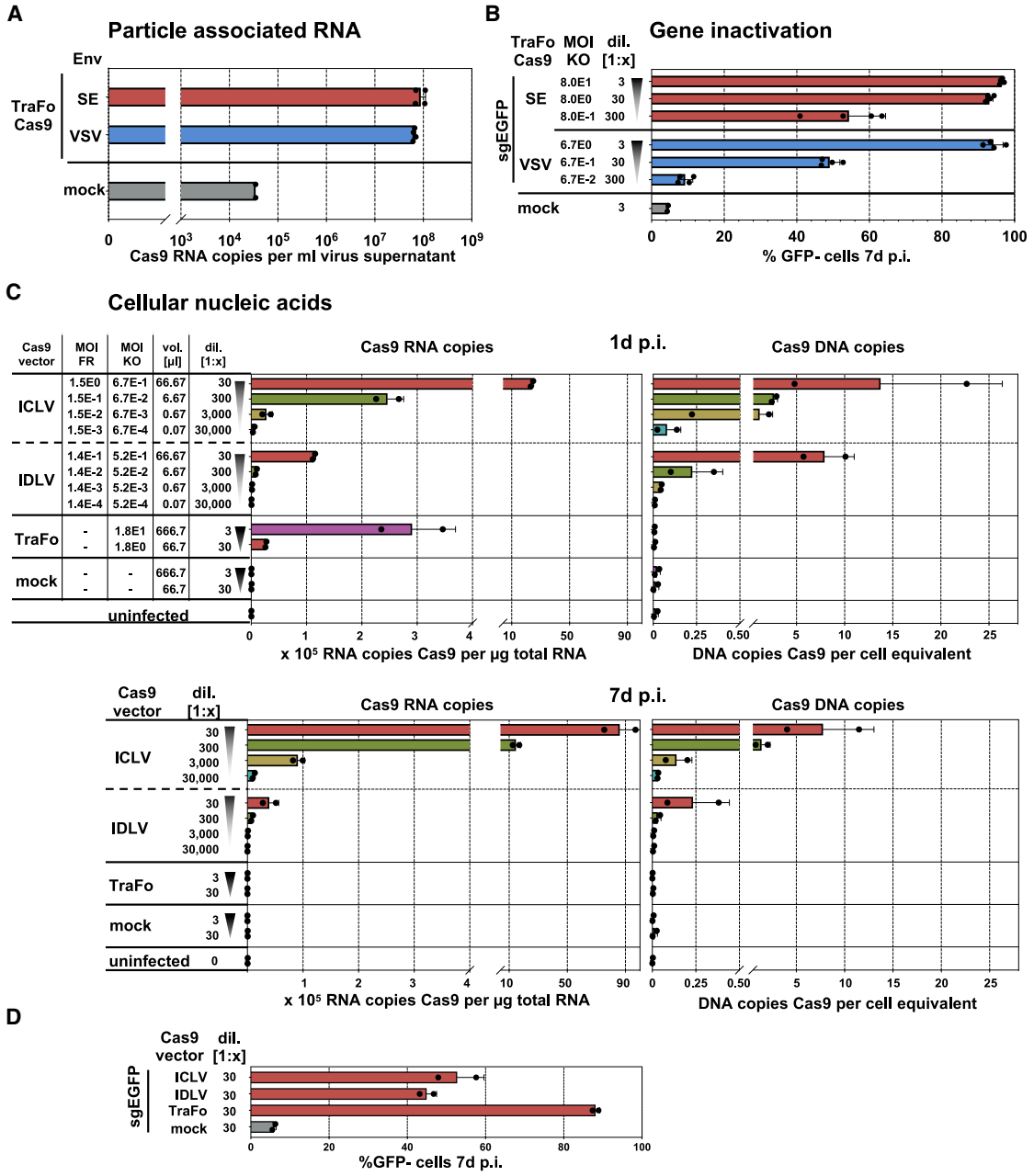

Figure 2. Absence of Cas9-Encoding DNA after TraFo-Cas9 Vector Transduction of Target Tissue

(A) TraFo-Cas9 particle supernatant nucleic acid analysis. *Cas9* mRNA copy numbers per mL plain TraFo vector supernatant harboring SFVmcy Env (SE) or VSV-G (VSV), as well as mock supernatant (mock; Cas9 RNA Transfer vector only without packaging plasmids) were determined by qPCR with a *Cas9*-specific primer probe set. Shown are means ± SD (n = 2, independently produced viral supernatants each as mean of two technical replicates). (B) *GFP* inactivation efficiencies on U2OS-GFP stably expressing an *egfp*-specific sgRNA (sgEGFP) mediated by different serial dilutions of the same virus supernatants analyzed in (A). (C) 5×10^4 U2OS-GFP cells, plated in 6-well plates 24 h in advance, were transduced in 2 mL total volume with TraFo-Cas9 (TraFo) or *Cas9*-encoding ICLV (ICLV) or IDLV (IDLV) vector supernatants at different dilutions (corresponding volumes of plain supernatants are given) as indicated. Alternatively, cells were incubated with the same concentrations of mock supernatants (mock) derived from 293T transfected with *Cas9* RNA transfer vector only without packaging plasmids or fresh growth medium (uninfected). At 3 days p.i., the multiplicity of infection for individual supernatants was calculated from either the frequency of a co-expressed fluorescent reporter (MOI-FR) or from the frequency of *GFP* inactivation (MOI-KO) on U2OS-GFP

(legend continued on next page)

(Figure 3C). In contrast, in mismatch sgRNA-expressing target cell populations (sgEGFPm1, m2), significant differences in the frequency of *GFP* inactivation were found between the three types of viral Cas9 delivery. ICLV-mediated delivery of Cas9 resulted in ≥65% of *GFP* KO even in the presence of mismatches in the sgRNA sequence at 8 days p.i. The same mismatches were tolerated less well by IDLVs. However, TraFo-Cas9 delivery displayed the highest sensitivity to mismatches, resulting in the greatest specificity in the respective target cell populations (sgEGFPm1, m2: ≤7% GFP KO). When determining the targeting specificity by calculating the ratio of *GFP* inactivation with sgEGFPwt over sgEGFPm1 or -m2 a slightly improved on-target specificity was measured for IDLV over ICLV Cas9 delivery for sgEGFPm1 (1.7×) and sgEGFPm2 (2.9×) (Figure 3D). However, for TraFo-Cas9 delivery on-target specificity was improved by one order of magnitude (sgEGFPm1: 10.1×, sgEGFPm2: 23.4×) compared to corresponding ICLVs. Moreover, on-target specificity after TraFo-Cas9 delivery was also greatly improved over IDLV Cas9 transductions (sgEGFPm1: 5.8×; sgEGFPm2: 8.0×). Furthermore, our fully transient TraFo-Cas9 delivery system did not show any loss in targeting specificity from day 3 to day 8 (Figure 3C), whereas a significant loss in targeting specificity over time was observed for ICLVs and for IDLVs.

Thus, transient expression of Cas9 by target cell transduction with mRNA containing TraFo-Cas9 particles efficiently induces DNA double-strand breaks and subsequent non-homologous end joining (NHEJ)-mediated gene inactivation, which not only in contrast to ICLVs but also IDLVs has a remarkably improved on-target specificity.

Detection of Residual Integration of Retroviral Vector Genomes

IDRV genomes, as well as other forms of episomal DNA, are known to possess a residual low-level non-integrase-mediated integration capacity.[39–42] Because the most promising two-virus CRISPR vector system employed either IDPV or ICPV vector genomes, we wanted to determine the level of residual integration of IDPV *sgRNA*-encoding genomes in U2OS-GFP cells. For that purpose, the PFV sgRNA vector genomes were amended by a *DsRed* expression cassette (Figure 3A). Furthermore, we generated similar IDLV based vectors to compare their gene inactivation and residual integration capacity to the corresponding PFV sgRNA-DsRed vectors. IDRV sgRNA-DsRed particles of PFV or HIV-1 origin were used in combination with TraFo-Cas9 particles to co-transduce U2OS-GFP cells (Figure 3E). GFP and DsRed fluorescence of transduced target populations was monitored by flow cytometry over time. The observed gene inactivation efficiencies recapitulated the results obtained with sgRNA vector particles without additional *DsRed* expression cassette (Figure 1A). Single exposure of U2OS-GFP cells or MEF-GFP to 1:1 mixtures of plain TraFo-Cas9 vector supernatants in combination with plain IDPV or IDLV sgRNA DsRed vector supernatants suggested a higher residual integration potential for IDLV than for IDPV at similar gene inactivation efficiency (Figure S3). However, this was the consequence of higher titers obtained for IDLVs, as revealed by further experiments with MOI adjusted PFV or HIV sgRNA-DsRed vector supernatants (Figures 3E and 3F). Here, IDLV-transduced samples displayed at 11 days p.i. a somewhat higher, but not statistically significant different, residual integration capacity than IDPV-transduced samples (IDPV, 6.1%; IDLV, 6.9%), while having a slightly lower overall gene inactivation efficiency (IDPV, 83.1%; IDLV, 78.8%) (Figures 3E and 3F). Taken together, our data suggest that IDLV and IDPV sgRNA vectors when combined with TraFo-Cas9 vectors confer comparable KO efficiencies and display a similar residual integration frequency of 7%–8% of the GFP− cell population.

TraFo-Cas9 Mediated T Cell Receptor Knock Out in Immortalized and Primary Human T Cells

Modified T cells expressing chimeric antigen receptors (CARs) can be redirected to mediate tumor rejection.[43,44] Great potential of CAR T cells for immunotherapy attracts strong interest for improved *CAR* transgene delivery and simultaneous genome engineering. Currently, delivery of *CAR* transgenes is based on lentiviral or gamma-retroviral vectors, and CRISPR/Cas9-induced genome editing mostly depends on electroporation of RNPs.[45] In order to examine the potential of TraFo-Cas9 delivery as an additional option for genome engineering of human T cells, we targeted the endogenous T cell receptor alpha constant (*TRAC*) locus. First, we tested three different *TRAC*-specific sgRNAs (sgTRACs) for their efficiency to accomplish stable *TRAC* inactivation after IDLV or ICLV transduction and TraFo-Cas9 codelivery in an immortalized human T cell line (Jurkat). A single coinfection of Jurkat cells with unconcentrated supernatants resulted in efficient gene disruption with combinations containing IDLV sgRNA vectors being only slightly less efficient than the respective ICLV combinations (Figures 4A and 4B). Depending on the applied sgTRACs, an average of 12.6%–57.4% for cotransduction with IDLVs and 19.3%–66.3% for ICLV coinfection did not show T cell receptor (TCR) cell surface expression in flow cytometry analysis at 7 days p.i.

For the next step, we chose the most promising sgTRAC (sgTRAC3) for application on primary human T cells. Several reports suggest that initial phase of transcription from retroviral genomes might take longer in primary human T cells than in common human T cell lines like Jurkat.[46–49] As a consequence, we decided to stably transduce primary cells with an expression cassette for sgTRAC transcription (with ICLVs) 1 day ahead of TraFo-Cas9 transduction. *De novo* sgRNA transcription from stable retroviral infections thereby keeps open the possibility of augmenting retroviral sgRNA vector genomes for additional expression of gene products (e.g., CAR) in the future. A

sgEGFP1 cells. In a separate experiment, cellular RNA and DNA was isolated from transduced U2OS-GFP cells at two different time points (1 day and 7 days p.i.). Shown are mean ± SD (n = 2, infections with independently produced viral supernatants each as mean of two technical replicates) of *Cas9* RNA copies per μg total RNA and *Cas9* DNA copies normalized for β-actin content. (D) *GFP* inactivation efficiency mediated by the same virus supernatants as shown in (C) at a 1:30 dilution on U2OS-GFP stably expressing an *egfp*-specific sgRNA (sgEGFP). Shown are mean ± SD (n = 2, infections with independently produced viral supernatants).

single incubation of primary human T cells (expressing sgTRACs) with TraFo-Cas9 supernatant disrupted TCR expression in approximately 20% of stably transduced cells (Figure 4C). Thus, TraFo-Cas9-mediated transient expression in primary human T cells in combination with stable sgRNA expression enables gene inactivation at a reasonable efficiency.

Gene Editing by TraFo-CRISPR/Cas9 Vectors

Following our finding, that the highest gene inactivation efficiencies could be achieved if TraFo-Cas9 vectors were combined with ICRV or IDRV sgRNA particles we wondered whether the sgRNA vector genome could be amended by a repair matrix to simultaneously enable homology directed repair (HDR)-mediated gene editing. This type of PFV CRISPR vector particle was termed sgRNA-HDR vector.

The gene-editing capacity of PFV sgRNA-HDR vectors was evaluated by establishing two variations of a color-switch assay using U2OS-GFP target cells. First, we used an HDR matrix consisting of a *T2A peptide-DsRed Express 2* (*T2A-DsRed*) ORF, lacking a translation start but containing a translation stop, which was flanked by 5′ left-hand homology region (LHR) and 3′ right-hand homology region (RHR) of different homology length (Figure 5). The repair matrix lacked the sgRNA *egfp* target sequence, making it resistant to CRISPR/Cas9 cleavage. HDR-mediated in-frame insertion of the *T2A-DsRed* ORF into the CRISPR/Cas9-induced DSB led to loss of GFP and gain of DsRed expression (Video S1). To avoid expression of DsRed by either episomal PFV vDNA or random chromosomal vDNA integration, we limited the LHR to 232 bp, terminating before the cytomegalovirus (CMV) promoter TATA box, whereas the RHR used was encompassing up to 2,123 bp (Figure 5). Following transduction of U2OS-GFP cells with combinations of plain TraFo-Cas9 and different IDPV sgRNA-HDR vector supernatants with varying homology arm length (Figure 5B), or ICPV sgRNA-HDR vector supernatants alone (Figure S4), GFP and DsRed expression was monitored at 10–11d p.i. No DsRed-expressing cells could be detected after transduction of target cells with ICPV supernatants of sgRNA-HDR vectors alone (Figure S4), or with a combination of TraFo-Cas9 and IDPV sgRNA-HDR vectors without homology regions (0–0) (Figure 5B). In contrast, all combinations with IDPV sgRNA-HDR viruses harboring homology regions of at least 50 bp length (50–50) did show DsRed expression most likely as a consequence of HDR-mediated editing of the *GFP* locus in U2OS-GFP cells. The longer the homology regions were, the higher was the HDR frequency achieved, resulting in up to 5.5% of $GFP^-/DsRed^+$ cells (232–2,123) in unselected, transduced U2OS-GFP cell populations.

Due to the lack of a functional promoter upstream from the *DsRed* ORF in the sgRNA-HDR vector genome, the level of its random integration and/or occurrence of incomplete HDR events could not be examined. Therefore, a variant sgRNA-HDR vector genome (LHR 232 bp and RHR 547 bp) was generated, which harbored downstream of the sgRNA expression cassette an additional promoter-driven near infrared fluorescent (*iRFP*) reporter gene, having no sequence homology to the DsRed Express 2 (*DsRed*) ORF of the repair template (Figure 6A). U2OS-GFP cells were transduced with respective IDPV sgRNA-HDR vector supernatant in combination with TraFo-Cas9 supernatant, followed by a three-color flow cytometry analysis. Inclusion of the *iRFP* expression cassette into the sgRNA-HDR vector genome did reduce the fraction of $GFP^-/DsRed^+$ cells from 4.59% to 3.42% (Figure 6B). However, it revealed that the majority (~75%) of all $GFP^-/DsRed^+$ cells were correct HDR events as they lacked iRFP expression (Figures 6B and 6C). In control samples of target cells that were transduced with identical amounts of respective ICPV supernatants without TraFo-Cas9 cotransduction >95% of the population expressed iRFP as a consequence of stable vector genome integration (Figure 6C; Figure S5A). At the same time the $DsRed^+$ fraction was at mock level (Figure S5A). This clearly demonstrates that the exclusive provision of the promoter-less repair template does not lead to efficient DsRed expression.

Furthermore, HIV-1 based IDLV sgRNA-HDR vector supernatants containing an analogous genome with *iRFP* expression cassette were included in the analysis for comparison. When identical amounts of plain IDLV vector supernatant were applied, they showed a 2-fold increase in $GFP^-/DsRed^+$ cell numbers in comparison to IDPV sgRNA-HDR particles, with both sample types having a similar fraction of $iRFP^-$ cells (75% of all $GFP^-/DsRed^+$ cells) (Figure 6B). The detailed characterization of target cell populations by three-color flow cytometry analysis demonstrated that the majority (~75%) of DsRed-expressing cells arising from co-transduction with TraFo-Cas9 vectors and either IDPV or IDLV sgRNA-HDR particles harbor correct HDR events (Figure 6B).

The second type of color-switch assay employed in our study was recently published.[50] Unlike inserting a whole additional ORF encoding a different fluorescent protein into another fluorescent protein ORF, this assay is based on a *GFP*-to-*BFP* conversion due to HDR-mediated gene editing introducing nucleotide exchanges into the *egfp* ORF. A PFV sgRNA-HDR vector with a *GFP-BFP* switch homology repair matrix upstream of a *egfp*-specific sgRNA expression cassette was generated (Figure 6D). In addition, a *DsRed* expression cassette was inserted, to enable detection of random IDPV genome integrations or incomplete HDR events. Co-infection of U2OS-GFP target cells with 1:1 mixtures of plain TraFo-Cas9 and IDPV sgRNA-HDR vector supernatants resulted in a *GFP* inactivation of up to 80% (Figure 6D). Simultaneously, more than 11% of the unselected, transduced cell populations showed a stable GFP to BFP (GFP^-/BFP^+) conversion (Figure 6D). Analysis of DsRed expression in the GFP^-/BFP^+ cell population revealed that only about 5% of the GFP^-/BFP^+ cells had additional random integrations of IDPV vector genomes or represented incomplete HDR events (Figure 6C). Transduction of U2OS-GFP cells with ICPV sgRNA HDR vector supernatant without co-transduction by TraFo-Cas9 confirmed that the *DsRed* expression cassette for negative selection is functional and the repair template alone does not result in efficient BFP expression (Figure 6D; Figure S5B).

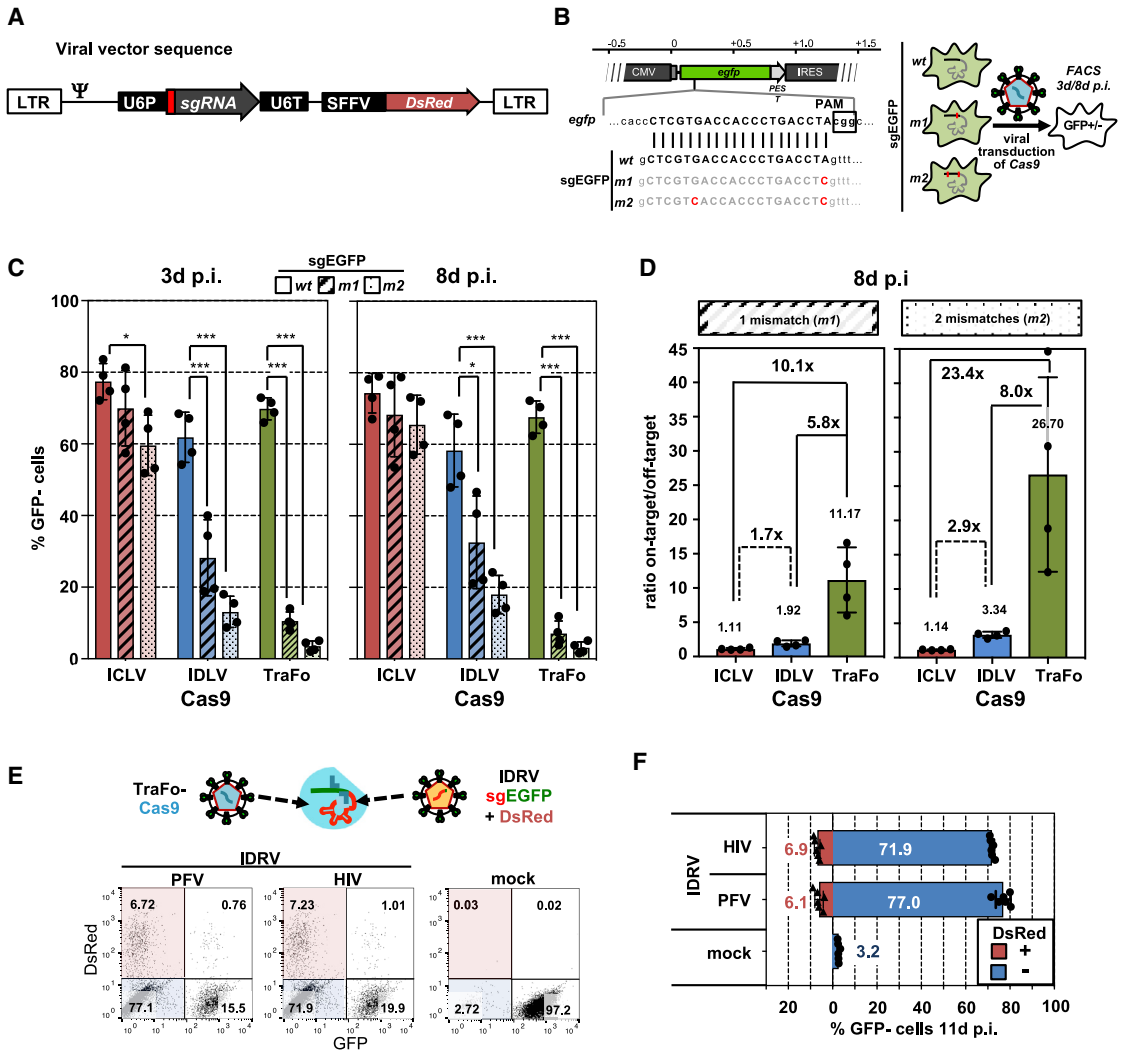

Figure 3. Analysis of TraFo-Cas9 Mediated Targeting Specificity and Residual Integration Efficiency of IDRV Genomes

(A) Schematic illustration of vector genome structure of PFV or HIV origin harboring U6 promoter-driven sgRNA expression cassettes, which were amended by a SFFV-U3 promoter-driven DsRed Express 2 (*DsRed*) reporter cassette. (B) Schematic illustration of the U2OS-GFP target locus, sgRNA specificities, and experimental design. The enlargement shows the target locus sequence in the *egfp* ORF PAM sequence. The targeting sequences of the different sgRNA variants are aligned. Mismatched residues in the sgEGFPm1 and m2 sgRNA variants are highlighted in red. The experimental design involved U2OS-GFP cell populations stably transduced with the individual sgRNA vectors and subsequent transduction with the different *Cas9*-encoding vector particles. (C) Flow cytometry analysis of *GFP* inactivation following transduction of U2OS-GFP cells, stably expressing the individual sgRNA species as indicated, with *Cas9* expressing integration-competent lentiviral vector (ICLV), integration-deficient lentiviral vector (IDLV), or TraFo-Cas9 vector supernatants at 3 days p.i. and 8 days p.i. Means ± SD (n = 4; infections with independently produced viral supernatants) of fraction of $GFP^{-}/DsRed^{+}$ cells are displayed (MOI-KO TraFo Cas9, 1.13 ± 0.13; IDLV, 0.90 ± 0.25; ICLV, 1.38 ± 0.21 determined on U2OS-GFP sgEGFPwt cells at 8 days p.i.). (D) On-target to off-target ratios for sgEGFP m1 and m2 sgRNA variants calculated from the data shown in (C). (E and F) U2OS-GFP target cells were transduced with TraFo-Cas9 virus supernatants in combination with different, MOI adjusted sgRNA-encoding ID retroviral vector supernatants of PFV and HIV origin as indicated on the y axis (MOI-FR IDPV, 0.87 ± 0.05; IDLV, 0.57 ± 0.08 calculated from DsRed expression 3 days p.i.). Mock, uninfected target cells. Flow cytometry analysis of GFP and DsRed expression was performed 11 days p.i. (E) Representative FACS dot blot profiles of transduced U2OS cell samples. (F) Means ± SD (n = 6; three infections with two independently produced viral supernatants) of fraction of GFP^{-} cells and distinguishing between DsRed expressing ($DsRed^{+}$, red bars) and non-expressing ($DsRed^{-}$, blue bars) fractions are displayed.

In a nutshell, transduction of target cells with IDPV sgRNA particles carrying an additional repair matrix in combination with TraFo-Cas9 vectors enables efficient gene editing with little off-target insertions. Introducing small point mutations instead of gene insertions at specific genomic loci appears to be more efficient and less error-prone.

Tagging of Endogenous Human Genes by TraFo-CRISPR/Cas9 Vector Transduction

To test our TraFo-CRISPR/Cas9 HDR vector system in a practical application, we developed a tagging system for endogenous genes. As a proof of principle, we decided to target the human polo-like kinase 1 (*PLK1*) gene locus with the TraFo-CRISPR/Cas9 vector system. Mediated by HDR, we wanted to specifically integrate a selection marker (puromycin) and an in frame N-terminal *GFP* tag upstream of the *PLK1* ORF leading to the expression of a GFP-PLK1 fusion protein (Figure 7A). To differentiate between GFP fluorescence resulting from specific HDR events and that arising from incomplete HDR events or randomly integrated sgRNA HDR vector genome integrations, we included an in-frame *DsRed* expression cassette downstream of the RHR in the sgRNA HDR vector genome (Figure 7A).

We first examined the targeting efficiency of four different sgRNAs specific for the 5′ region of the first *PLK1* exon (Figure S6A). Genomic DNA of HeLa cells was isolated 3 days after a single transduction with our Two-Virus system consisting of TraFo-Cas9 and the different *PLK1*-specific sgRNA IDPVs lacking a repair matrix. A T7 endonuclease assay demonstrated efficient target cleavage and did not reveal significant differences in the efficiency between the four *PLK1*-specific sgRNAs tested (Figure S6B). Subsequently, we used two *PLK1*-specific vectors (sgPLK1-1 and sgPLK1-4) or one Ctrl (sgCtrl) sgRNA-HDR IDPV vector that contained an appropriate *PLK1* repair matrix (Figure 7A) each in combination with TraFo-Cas9 vector particles to transduce HeLa cells.

For all transduced samples, GFP^+ cells were detectable in unselected cultures at 4 and 8 days p.i., with the fraction of *GFP*+ cells being significantly higher in samples that received *PLK1*-specific sgRNAs than in Ctrl sgRNA samples (Figure S6C). Although IDPV sgRNA-HDR particles were employed, puromycin-resistant cell populations were obtained by drug selection for all samples incubated with TraFo-Cas9 supernatant together with sgRNA-HDR vector particles, including sgCtrl-HDR samples. However, sgCtrl-HDR samples had a much larger fraction of DsRed-expressing cells than samples transduced with *PLK1*-specific sgRNA-HDR vector particles (Figure 7B), suggesting that HDR-mediated knock in results in the loss of the non-homologous negative selection marker DsRed.

The PLK1 protein is naturally expressed in a cell-cycle-dependent manner with the *PLK1* promoter being most active during S-G2-M phase.[51,52] Hence we attempted to increase the *PLK1* promoter-dependent expression by arresting cells in mitosis by the addition of nocodazole. Furthermore, $DsRed^-$ cells with low GFP expression were enriched by cell sorting from nocodazole-arrested cultures co-transduced with TraFo-Cas9 and either of the two *PLK1*-specific sgRNA-HDR vectors (Figure 7B). Subsequently, genomic DNA isolated from these different HeLa cell subpopulations, as well as respective parental cell populations, were analyzed by qPCR (Figures 7A and 7C). Only in samples where Cas9, *PLK1*-specific sgRNAs and repair matrix were provided by viral transduction could specific HDR events be detected. Furthermore, enriched cell populations with low GFP and no DsRed fluorescence showed 2.5 to 5.9 times more HDR-mediated correct integrations than their unsorted parental counterparts.

Additionally, a protein with the molecular weight of the expected GFP-PLK1 fusion protein could be verified by western blot analysis only in lysates of cells transduced with locus-specific sgRNA-HDR vectors, both with a GFP- and PLK1-specific antibody (Figure 7D). Furthermore, the amount of DsRed protein was strongly reduced in cell lysates, where specific sgRNA-dependent DNA cleavage and subsequent HDR could take place (Figure 7D, lanes 2 and 3). Sorted cells with low GFP and no DsRed signal (Figure 7D, lanes 6 and 7) showed the highest GFP-PLK1 expression level and no presence of the DsRed protein in western blot analysis. Taken together, these data are in line with the qPCR analysis of HDR frequency and suggest that the $GFP^+/DsRed^-$ cell populations have a significant enrichment in correct HDR events.

Finally, after proving the expression of the fluorescently tagged PLK1 protein by western blot, we examined the spatiotemporal distribution of GFP-PLK1 fusion proteins by confocal fluorescence microscopy analysis. Due to the qPCR and western blot analysis described above, we particularly focused on sorted cells with GFP and no DsRed expression. The analysis revealed that subcellular localization of the GFP signal in sgRNA-HDR vector-targeted cell populations (TraFo-Cas9 + IDPV sgPLK1-HDR) perfectly reflected the natural subcellular distribution for the PLK1 protein described in the literature[51,52] (Figure 7E). Furthermore, no DsRed signal was detectable in these cells (data not shown) and the GFP fluorescence intensity was dynamic and peaked in mitotic cells. In contrast, cells of a control population that was transduced with a integration-competent sgRNA HDR vector genome only (ICPV sgPLK1-1-HDR), resulting in random chromosomal integration of vector genome in the absence of Cas9 co-expression, did express DsRed and displayed a diffuse, homogeneous distribution of the GFP signal within the cell (Figure S7).

DISCUSSION

The adaptation of the bacterial CRISPR/Cas9 system has and is still revolutionizing genome engineering and has opened up entirely new possibilities for numerous *in vitro* and *in vivo* applications. However, major safety concerns about genome editing through CRISPR/Cas9 are still present. Well-established methods of Cas9 (and repair matrix) delivery often harbor risks like permanent integration of CRISPR/Cas9 expression cassettes, unintentional off-target mutations, or illegitimate homology-directed repair, which are difficult to control.

Particularly with regard to clinical applications, Cas9 target specificity often is a significant limitation, which appears to be strongly influenced by the level and duration of CRISPR/Cas9 availability in target tissues. Furthermore, prolonged expression of Cas9 and sgRNA may decrease fitness of edited cells and cause tissue damage, posing another restriction for clinical applications.[53,54] Therefore, transient

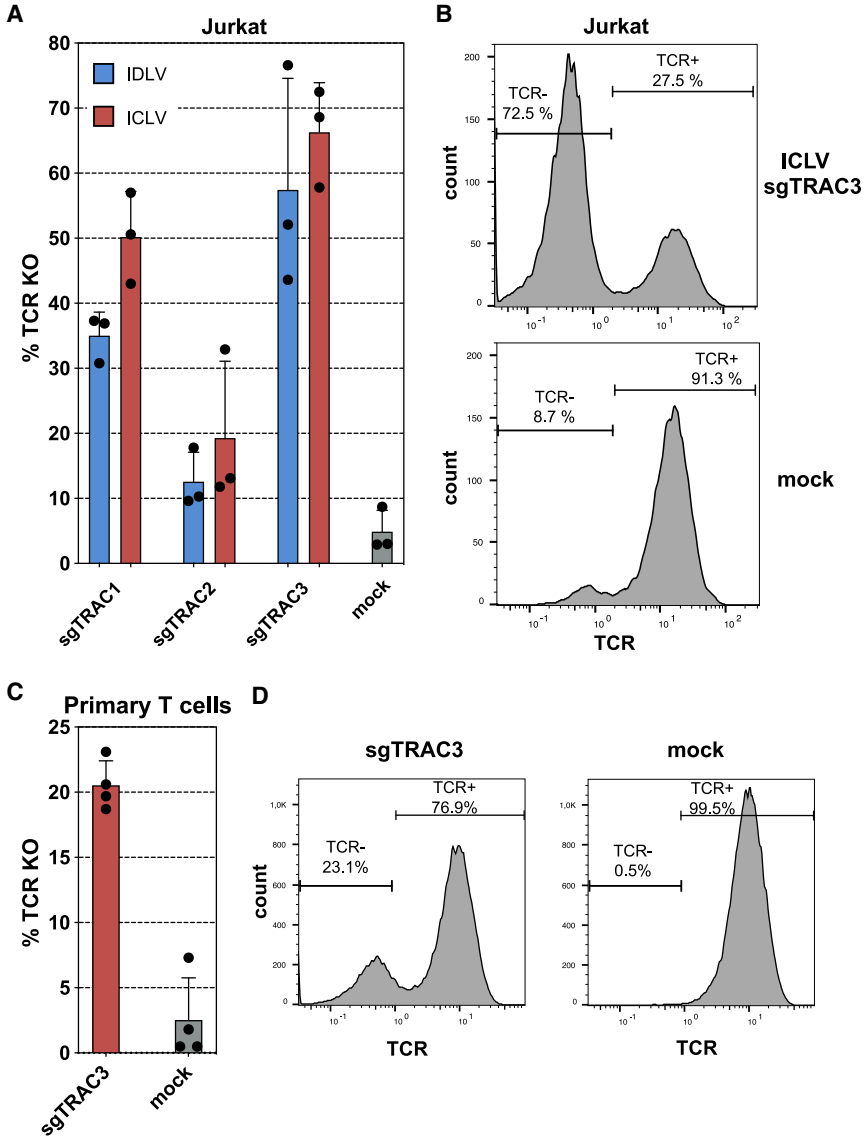

Figure 4. Knock Out of T Cell Receptor in Jurkat Cells after TraFo-Cas9 Transduction

2×10^5 Jurkat cells were transduced in 48-well plates with VSV-G pseudotyped IDLV or ICLV supernatants providing T cell receptor alpha constant locus specific sgRNAs (sgTRACs) together with TraFo-Cas9 particles at a 1:4 ratio in 500 µL total volume (MOI-FR ICLV, 0.96 ± 0.12; IDLV, 0.05 ± 0.01; determined on U2OS-GFP cells 3 days p.i.; MOI-KO TraFo-Cas9 KO, 1.51 ± 0.01, determined on U2OS-GFP cells 4 days p.i.). FACS analysis of cell surface TCR expression of infected Jurkat cells was conducted at 7 days p.i. (A) Means ± SD (n = 3, independent transductions with independently produced viral supernatants) of cell surface TCR KO as a consequence of *TRAC* inactivation using the individual *TRAC*-specific sgRNAs, as indicated. (B) Representative histograms of pan-TCR α/β antibody staining of Jurkat cells. (C) 5×10^5 primary human T cells were stably transduced with VSV-G pseudotyped ICLV supernatants of sgTRAC3 (MOI-FR: 23.2 ± 1.8) one day ahead of TraFo-Cas9 (MOI KO, 8.74 ± 0.23 – 20.8 ± 2.6) transduction. Cell surface TCR expression was analyzed at 7 days p.i. using flow cytometry. Means ± SD (n = 4, independent transductions with independently produced viral supernatants). (D) Representative histograms of pan-TCR α/β antibody staining of primary human T cells.

expression systems in particular of Cas9 might constitute a very promising approach to counteract these limitations.

Viral transduction of CRISPR/Cas9 components with IDLVs and subsequent gene inactivation is known to be efficient in a variety of cell types and tissues. However, viral integrase-independent genomic integration of viral vector DNA, which is to a certain extent unavoidable, does not make IDLVs a fully transient delivery system.[20,39,40,55,56] In addition, HDR-mediated knock in of lentiviral-transduced repair matrices is prone to illegitimate recombination and the formation of concatemers.[17,57,58]

We wanted to establish a method of retroviral CRISPR/Cas9 delivery, which addresses both problems—target specificity and unintended DNA integration of CRISPR/Cas9 components. With the TraFo-CRISPR/Cas9 system described in this study, we provide the Cas9 protein and the accompanying sgRNA separately by two different vector particles. We took advantage of the recently described unique PFV characteristic to efficiently transduce non-viral RNAs.[35] It enabled us to deliver an mRNA transcript encoding *Cas9* (TraFo-Cas9) and thereby transiently provide the endonuclease in target cells. This resulted in an efficient gene inactivation by error-prone NHEJ if specific sgRNAs were present in sufficient amounts in target cells. The latter was achieved best in combination with ICRV or IDRV particles containing a U6 promoter-driven sgRNA expression cassette. Addition of TraFo-Cas9 vector amounts corresponding to 60 copies *Cas9* mRNA per U2OS-GFP cell was sufficient to enable highly efficient *GFP* KO (>80% GFP^- cells). KO efficiencies achieved by the combination of TraFo-Cas9 and IDPV sgRNA particles are similar to those reported by Zuris et al.[59] using an optimized RNP transfection protocol with the same U2OS-GFP assay system and an identical *egfp*-specific sgRNA.

To apply the system in a practical translational setting, we examined the efficiency of *TCR* KO by simultaneous TraFo-Cas9 and ICLV/IDLV sgTRAC transduction. Simultaneous incubation of Jurkat T cells with plain TraFo-Cas9 and ICLV/IDLV sgRNA particle supernatant resulted in efficient *TCR* KO (ICLV, 66.3%; IDLV, 57.4%).

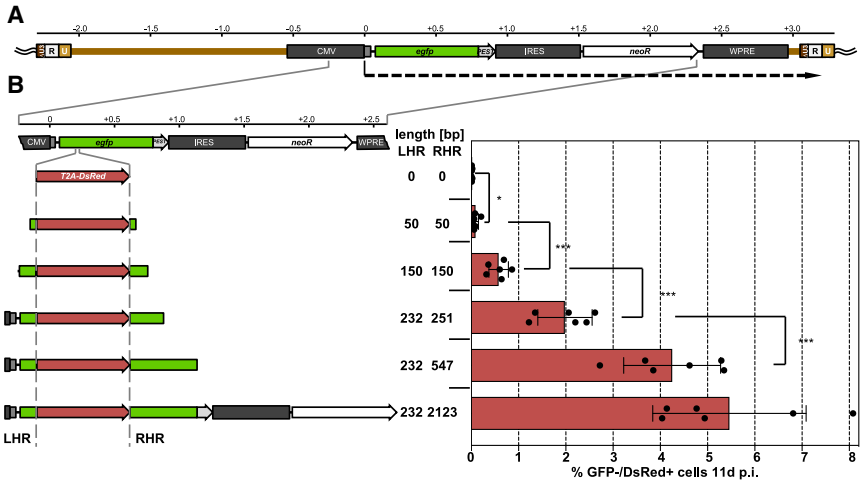

Figure 5. HDR-Mediated Gene Insertion Using CRISPR/Cas9 Two-Virus Vectors

U2OS-GFP target cells were co-transduced with plain, cell-free supernatants of TraFo-Cas9 vectors and the different IDPV sgRNA-HDR vectors, containing *GFP* target locus specific homology arms of variable length, as indicated, at a 1:1 ratio in 1 mL total volume. (A) Schematic illustration of the *GFP* target locus structure of U2OS-GFP cells representing a single lentiviral proviral vector genome harboring a CMV promoter-driven expression cassette for a destabilized GFP and neomycin resistance protein. (B) Influence of homology arm length. Flow cytometric analysis of GFP and DsRed expression of U2OS-GFP target cells at 11 days p.i. with two-virus PFV vector supernatant combinations containing different sgRNA-HDR vector genomes. Means ± SD (n = 6; infections with independently produced viral supernatants) of the percentage of *GFP*$^{-}$/*DsRed*$^{+}$ target cells are displayed. The length of left-hand (LHR) and right-hand (RHR) homology arms flanking the *T2A-DsRed* ORF in the individual sgRNA HDR vector genomes is indicated on the y axis of the graph. To the left a graphical illustration of the repair matrix contained within the individual IDPV sgRNA-HDR vector genome is shown with an enlargement of the *GFP* target locus of U2OS-GFP cells on top.

These results encouraged us to also employ our system on primary human T cells. Our initial experiments on primary human T cells, as well as the results of others,[46] suggested that stable expression of sgRNA transcripts from retroviral vector genomes appears late at 3 days p.i. We have therefore decided to use ICLV particles to achieve stable sgTRAC expression. Incubation of cells with TraFo-Cas9 supernatant 1 day after ICLV sgTRAC transduction resulted in *TCR* KO in approximately 20% of the cell population demonstrating that the gene editing mediated TraFo-Cas9 delivery is also feasible for primary target tissues, although in this setting provision of the sgRNA in sufficient amounts appears to be the limiting factor and a transient sgRNA delivery by the TraFo system requires further improvements. Infections with TraFo-Cas9 supernatant at later time points after sgRNA vector transduction combined with a second restimulation of primary T cells, or improvement of the gene editing efficiency of a pure TraFo-Cas9/sgRNA delivery system (as discussed below), might help to further improve the efficiency of *TCR* KO in primary cells. Furthermore, other groups have already shown that corresponding ICLV vector genomes can be augmented to achieve simultaneous transgene expression, e.g., modification of human T cells with a chimeric antigen receptor to provide an artificial antigen specificity.[46] This may be an alternative as long as fully transient sgRNA provision at sufficient levels has not been implemented and CAR expression from a randomly genomic integrated additional transgene cassette is used and not a HDR-mediated replacement of endogenous *TCR* genes by *CAR* coding sequences.[60]

In U2OS-GFP cells, an entirely transient RNA delivery of both CRISPR/Cas9 components by combining TraFo-Cas9 and TraFo-sgRNA vector particles also resulted in a notable amount of specific gene inactivation events. Even though it required sequential application of the two TraFo vector particles (Cas9 and sgRNA) and was less efficient than sgRNA delivery by ICRV or IDRV transduction, it represents a promising approach solely making use of the TraFo system. At the moment, we do not know the exact restrictions responsible for the lower gene-editing efficiency of a pure TraFo-Cas9/sgRNA vector system. We suspect that one of the limitations responsible might be the nature of sgRNA expression in packaging cells. RNA polymerase III (Pol III) transcripts derived from U6 promoters are not actively exported from the nucleus as opposed to Pol II transcripts.[61] This may result in low cytoplasmic sgRNA levels or an intracytoplasmic sublocalization of sgRNAs, which is unfavorable for microtubule-organizing center-associated particle assembly of FVs. Vector particle concentration, an adjusted sgRNA design (as discussed below), or an alternative sgRNA expression approach (e.g., T7 RNA polymerase-mediated[62]) resulting in higher cytoplasmic levels of sgRNA in packaging cells could be helpful strategies to further improve gene inactivation efficiencies achieved by pure TraFo-Cas9 and TraFo-sgRNA transduction.

Remarkably, off-target analysis demonstrated a significantly reduced tolerance for sgRNA mismatches in target cells after TraFo-Cas9-mediated mRNA transduction versus IDLV-mediated transient or ICLV-mediated stable Cas9 delivery. Interestingly, the enhancement in targeting specificity was not associated with a reduction in targeting efficiency. These findings are in good agreement with observations made by others, showing that the implementation of methods for transient Cas9 transduction significantly improves on-target/off-target-ratios.[11,15,16,23,63] In addition and in contrast to IDLV-mediated Cas9 transduction, TraFo-Cas9 transfer is safe from the risk of insertional mutagenesis. Due to its transcription-independent nature, TraFo-Cas9-mediated expression might additionally be less prone to tissue- or species-specific negative influences.[15] We suggest that transient Cas9 target cell expression by TraFo-Cas9 transfer represents an attractive, efficient, and safe alternative to currently available retroviral delivery tools. In addition, TraFo-Cas9 transduction could

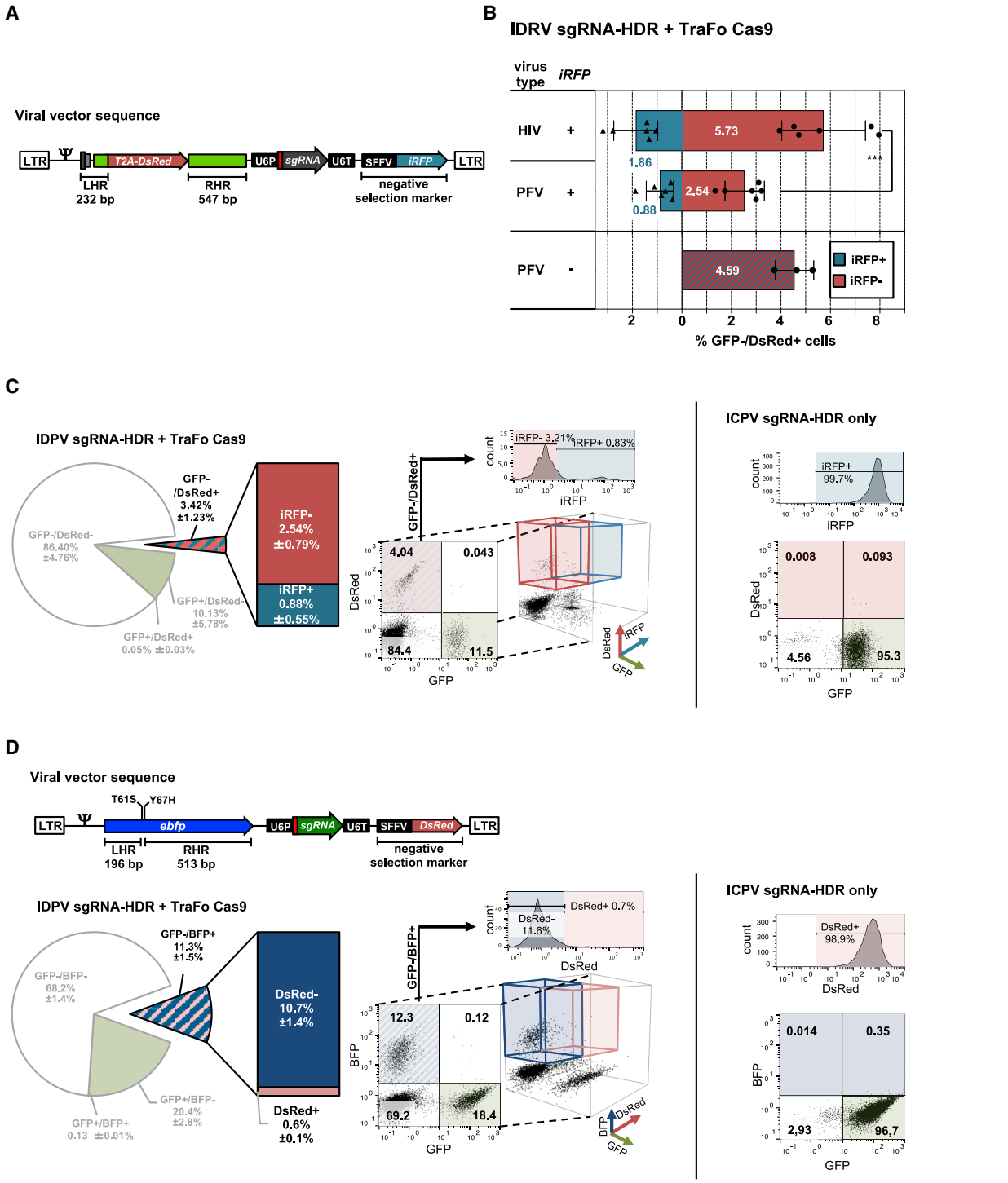

Figure 6. Efficient and Seamless Gene Editing by Two-Virus PFV CRISPR/Cas9 HDR Vector Systems

U2OS-GFP target cells were co-transduced with TraFo-Cas9 vector supernatants and different ID sgRNA-HDR vector particles of PFV (PFV) or lentiviral (HIV) origin, with (+) or without (–) additional *iRFP* reporter cassette, as indicated. (A) Schematic illustration of sgRNA-HDR vector genomes of PFV or HIV origin harboring a *T2A-DsRed* repair matrix, a U6 promoter-driven sgRNA expression cassette, and amended by a SFFV-U3 promoter-driven *iRFP670 (iRFP)* reporter protein expression cassette. (B) Comparison of various ID sgRNA-HDR vector particles. Flow cytometric analysis of GFP, DsRed, and iRFP expression of transduced U2OS-GFP target cells (11 days p.i). Graphical illustration of means ± SD (n = 6; independently produced viral supernatants) of the percentage of individual target cell populations are displayed (MOI-FR IDPV,

(legend continued on next page)

be a promising and broadly applicable alternative to ribonucleoprotein transfection or nanoparticle-mediated delivery of *in vitro* transcribed *Cas9* mRNA.

During the preparation of this manuscript, Knoop et al.[64] and Lu et al.[65] described similar murine leukemia virus- (MLV) and HIV-based CRISPR/Cas9 mRNA delivery systems. Both systems make use of additional aptamer stem-loops in their encapsidated *Cas9* mRNA molecules and aptamer binding proteins (MCP, MS2 coat protein; PCP, PP7 coat protein), either replacing the MLV NC peptide as a whole[64] or inserting it into the nucleocapsid (NC) peptide of HIV.[65] These structural requirements for effective RNA delivery with either HIV- or MLV-derived particles fit well to our previously published data, as we observed a still unspecified natural ability of PFV to transfer non-viral RNA significantly more efficiently than all other retroviruses tested so far.[35]

Lu and colleagues showed efficient delivery of CRISPR components by a simultaneous infection of target cells with IDLVs for sgRNA delivery and modified lentivirus-like bionanoparticles (LVLP) for aptamer stem-loop-mediated *Cas9* mRNA transduction, which follows a similar principle as our TraFo FV CRISPR vector system. Strikingly, the alternative retroviral RNA delivery system for CRISPR/Cas9 components of Knopp et al.[64] based on MLV enabled an RNA-only all-in-one gamma-retroviral platform for CRISPR/Cas9 transduction. However, unlike our TraFo-Cas9 system, efficient gene inactivation by this MLV vector system required in addition to inclusion of aptamer stem-loop sequences in *Cas9* and *sgRNA*-encoding RNAs concentration of viral supernatants. Interestingly, delivery of *Cas9-aptamer* and *sgRNA-aptamer* RNAs in separate MLV particles, instead of all-in-one particles, resulted in strongly diminished gene inactivation frequencies for unclear reasons, which is similar to what we observed for a pure transient FV RNA transfer CRISPR vector system when combining TraFo-Cas9 and TraFo-sgRNA particles. This may suggest that gene inactivation mediated by the RNA-only all-in-one MLV vector system is not solely the consequence of transduced RNA sequences (encoding *Cas9* and *sgRNA*) and, in case of *Cas9*, their *de novo* translation. Instead, functional RNPs might have already assembled in the packaging cell and thereby could have been delivered in all-in-one MLV particles via sgRNA-aptamer stem-loop interactions with MLV Gag-MCP. Such RNP delivery into target cells may significantly contribute to the gene inactivation efficiency achieved by this system. Indeed, transfer of RNPs by selective binding and incorporation of sgRNA-aptamers (as part of RNP complexes) into lentiviral particles was recently reported[66] and could also represent a promising option for an FV-based all-in-one RNP transfer system.

In contrast, the split-virus design of the PFV-based CRISPR delivery system presented in this study results in the independent transduction of *Cas9* and *sgRNA*-encoding sequences. While an all-in-one delivery system offers several advantages, especially in the case of poor cell transduction or the need of completely transient expression of all CRISPR components, its packaging capacity is limited. In contrast, our split-virus design created spare packaging capacity in the IDRV sgRNA genome, which could be exploited in various ways. For example, it permitted the addition of expression cassettes encoding negative selection markers (e.g., a fluorescent protein) to visualize and quantify cells with unintended and incorrect DNA integrations. By this we observed that sgRNA expression cassettes delivered by IDLVs or IDPVs led to residual vector genome integration in ~8% of transduced cells and was associated with similar gene inactivation efficiencies. We assume that such integrase-independent DNA integration of IDRV genomes occurs primarily at DSB sites. This is supported by the observation that the integration of IDLV vector genomes has molecular features reminiscent of those also described for other types of episomal DNA, such as plasmids, whereas ICLVs preferably integrate in lightly packed euchromatic genome regions.[39] Thereby IDLVs, similar to AAVs, also represent well-suited tools for detecting DNA cleavage.[56,67] Furthermore, as previously reported,[48,49] we also observed in this study a stimulatory effect of Cas9-mediated DNA cleavage on viral integration-independent DNA integration[48,49,55,56] (Figure S8). This observation further reveals that the integration frequency of IDRV genomes is markedly influenced by the availability of DSB sites, which in our opinion indicates preferred integration in genomic regions where free DNA ends are available.

Due to the split-virus design, it was also possible to simultaneously provide an additional DNA repair matrix with the sgRNA vector genome. Thereby, the TraFo-CRISPR/Cas9 vector system could be augmented further for application in HDR-mediated gene editing. The requirements and efficiency of gene editing by using such sgRNA-HDR vector genomes was examined in two different

3.78 ± 0.15; IDLV MOI, 13.48 ± 8.52 calculated from iRFP expression 2 days p.i.). (C) Three-color flow cytometry analysis of transduced U2OS-GFP populations. Shown is a pie chart diagram with means ± SD (n = 6; infections with independently produced viral supernatants) of the relative distribution of the four possible *GFP/DsRed* cell populations in the U2OS samples 11 days p.i. after TraFo-Cas9 and IDPV sgRNA-HDR vector co-transduction. For the *GFP*$^-$/*DsRed*$^+$ population the ratio of *iRFP*$^+$ to *iRFP*$^-$ subpopulations are indicated as bars. To the right, a representative three-dimensional point cloud of an individual cell population is shown. The individual fluorescence channels are each assigned to one axis of the cube. Far to the right a representative dot blot (GFP-DsRed) and histogram (iRFP) of a cell population transduced only by ICPV sgRNA-HDR vectors are shown. (D) Illustration of the PFV sgRNA-HDR vector genome harboring a *GFP-BFP* repair template, as well as U6 promoter-driven sgRNA and SFFV U3 promoter-driven *DsRed* reporter expression cassettes. Three-color flow cytometry analysis of transduced U2OS-GFP populations. Shown is a pie chart diagram of the relative distribution of the four possible *GFP/BFP* cell populations in U2OS samples 5 days p.i. For the *GFP*$^-$/*BFP*$^+$ population, the ratio of *DsRed*$^+$ to *DsRed*$^-$ subpopulations are indicated as bars. Means ± SD (n = 4; infections with independently produced viral supernants) of the percentage of individual cell populations are shown. To the right, a representative cell population is shown as a three-dimensional point cloud. The individual fluorescence channels are each assigned to one axis of the cube. A representative dot blot (GFP-BFP) and histogram (DsRed) of a cell population transduced only by ICPV sgRNA-HDR vectors are shown further to the right (MOI-FR IDPV, 2.80 ± 0.71 calculated from DsRed expression 2 days p.i.).

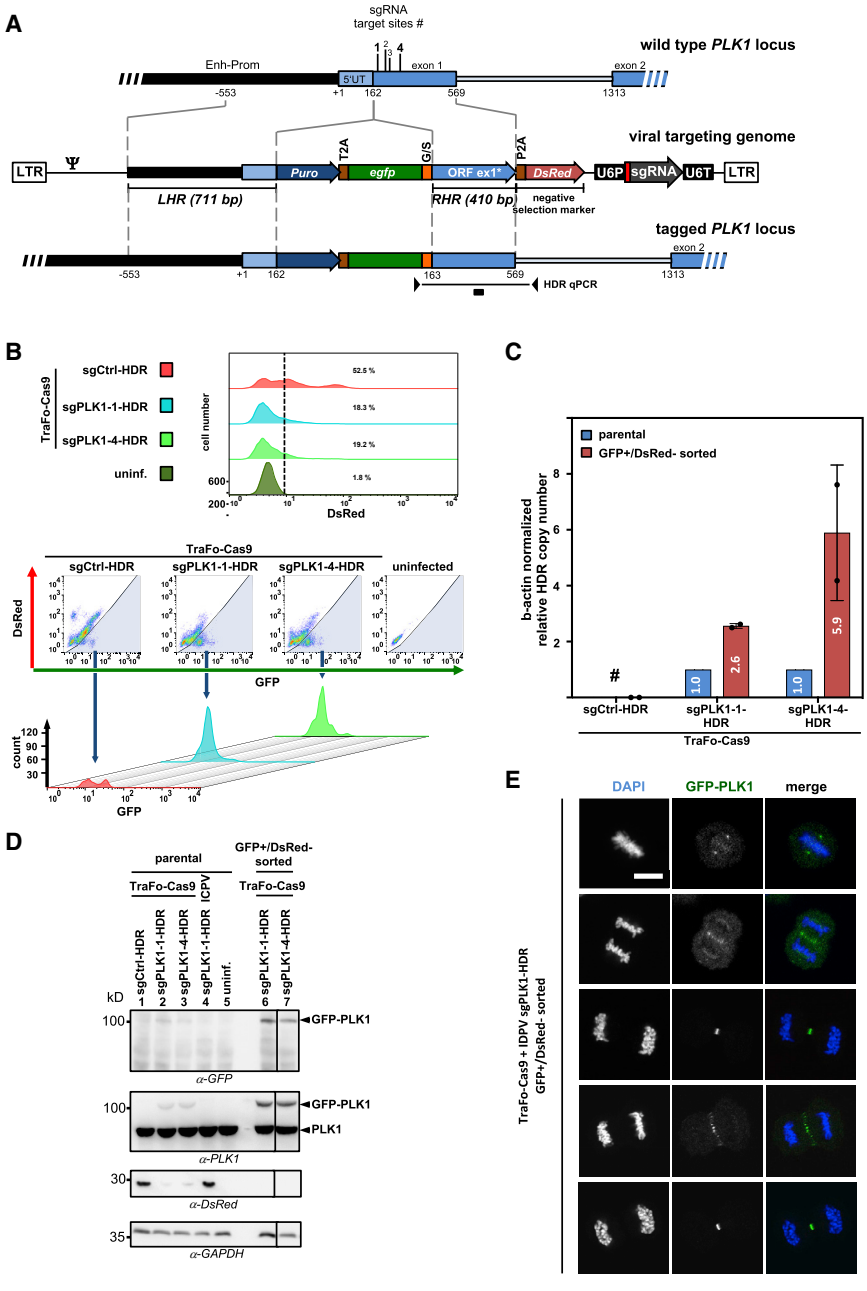

Figure 7. HDR-Mediated Tagging of Endogenous *PLK1* Using Two-Virus PFV CRISPR/Cas9 HDR Vectors

HeLa Kyoto target cells were co-transduced with TraFo-Cas9 vector supernatants and the different PLK1 sgRNA-HDR IDPV vector supernatants as indicated. (A) Schematic outline of the human *PLK1* locus and the PFV sgRNA-HDR proviral genome structure. *PLK1* exons are indicated as boxes with light blue (non-coding) or dark blue color (coding). Four different *PLK1*-specific sgRNAs target sites are marked, which were functionally evaluated in advance (Figures S6A and S6B). The repair matrix contains an ORF encoding a puromycin resistance-T2A-EGFP-$(G_4S)_3$ linker protein tag. It is flanked by a 711 bp LHR and 410 bp RHR with 3′ in frame fusion of a *P2A-DsRed Ex2* ORF. The primer-probe binding sites for the HDR-specific qPCR analysis are shown on the bottom. (B) Flow cytometry analysis of HeLa populations co-transduced with TraFo-Cas9 and different IDPV sgRNA-HDR vector supernatants (sgPLK1-1, sgPLK1-4, sgCtrl) or uninfected controls. Dot blots of GFP versus DsRed expression profiles of cell populations enriched by puromycin selection for 11 days and treated for 12 h with 0.1 μg/mL Nocodazole are shown. Histograms of DsRed fluorescence profiles of all cells are illustrated above. GFP histograms of depicted (blue) cell populations are shown below. Flow cytometry analysis of unselected, parental cell populations is shown in Figure S6C. (C) Analysis of HDR frequency in HeLa subpopulations by locus-specific qPCR. Genomic DNA isolated from parental (parental), as well as sorted HeLa cell subpopulations (*GFP*$^+$*/DsRed*$^-$ sorted), transduced with IDPV sgCtrl-HDR, sgPLK1-1-HDR, or sgPLK1-4-HDR in combination with TraFo-Cas9 vector supernatants were subjected to a qPCR analysis using a HDR-specific primer-probe set. Shown are means ± SD (n = 2) HDR copy numbers normalized for *β-actin* copy numbers relative to the level detected in parental cell populations. In genomic DNA from sgCtrl-HDR vector co-transduced cells, HDR copy numbers were below the detection limit of the qPCR analysis (#). (D) Western blot analysis of PLK1 expression. Protein lysates of parental or sorted (*GFP*$^+$*/DsRed*$^-$) HeLa cell populations transduced with various combinations of TraFo-Cas9 and IDPV sgCtrl-HDRs as indicated were subjected to western blot analysis using GFP-, PLK1-, or GAPDH-specific antibodies. Lane 4 represents a lysate of puromycin selected, parental HeLa cells transduced with ICPV sgPLK1-1-HDR (sgPLK1-1-HDR ICPV) vector supernatant alone. The identity of individual proteins is given to the right and molecular size markers to the left. The expected size of the PLK1 protein was 68.3 kDa. The GFP-PLK1 fusion protein was expected with a size of 96.8 kDa. (E) Confocal fluorescence micrographs of individual cells of HeLa TraFo-Cas9/IDPV sgPLK1-1-HDR *GFP*$^+$*/DsRed*$^-$, HeLa TraFo-Cas9/IDPV sgPLK1-4-HDR *GFP*$^+$*/DsRed*$^-$ cell populations showing the subcellular localization of the GFP signal during mitosis or interphase. Scale bar, 10 μm. Micrographs of ICPV sgPLK1-1 HDR transduced cell population are shown in Figure S7.

color-switch assays. Detection of HDR events required the presence of sequences homologous to the target locus. HDR targeting frequency increased with the length of the homology arms. In addition, introduction of point mutations was more efficient than gene insertions with observed HDR frequencies of up to 12% and 5%, respectively, without need for any enrichment procedures for viral supernatants or HDR events.

Differences between target cells, specific loci of DNA-cleavage, and/or DNA-repair and necessary methodological adjustments allow comparisons between different CRISPR/Cas9 delivery platforms only to a limited extent. For the GFP-BFP color-switch assay, we have re-sorted to a previously described sgRNA and previously used point mutations in the repair template.[50] Glaser et al.[50] reported a HDR frequency of up to 10%–12% of the edited cell population (HDR + NHEJ

subpopulations) using electroporation to cotransfect a double-stranded PCR repair template together with sgRNA/Cas9 expression plasmids. This is very similar to the HDR frequency we achieved by the TraFo-Cas9/IDPV delivery platform of 11% in unselected target cells, which corresponds to 14% of the edited cell population. We did not study the frequency of Cas9-induced off-target DNA cleavage in this assay, but as there are several indications of reduced off-target effects in transfections of *Cas9* mRNA compared to transfections of *Cas9*-encoding DNA plasmids,[15] we would suspect our TraFo-Cas9 system to also have certain on-target advantages over Cas9 expression via plasmid transfections.

Especially the locus-specific integration of longer DNA sequences mediated by HDR is known to be susceptible to errors.[17,57,58] IDRV delivery of HDR repair matrices can cause false or incomplete HDR events, induce the formation of concatemers or lead to a combination of both.[17] However, with our TraFo-Cas9 system, the packaging capacity of sgRNA-HDR vectors was not fully exploited, so we could add a negative fluorescence marker to visualize such undesirable genetic modifications. For transductions with sgRNA-HDR vectors of HIV or PFV origin, a frequency of about 25% incorrect DNA integrations in cells displaying a HDR-mediated color change from GFP to DsRed was observed. Additionally, we found HDR-mediated locus-specific gene insertions of longer sequences (*DsRed*) to be more error-prone (~25% unintended and/or incorrect DNA integration) than single nucleotide substitutions (GFP-BFP conversion: ~6% unintended and/or incorrect DNA integration).

Finally, we could show that the TraFo-Cas9 vector system is also applicable to tagging of an essential endogenous protein by adding a GFP-tag to the important cell-cycle regulator protein PLK1. Furthermore, by exploiting the inclusion of a negative selection marker (DsRed) in the repair matrix, it was possible to substantially enrich the number of correct HDR events for GFP-tagged PLK1 protein, by sorting against the expression of the negative selection marker.

At the moment, the combination of Cas9-sgRNA RNPs and AAVs encoding the repair template probably represent the safest delivery system for HDR strategies in human gene therapy.[68] If sorting against a negative selection marker is not an option, we think our TraFo-Cas9 delivery system could still represent an interesting alternative. Thereby, transduction of the long *Cas9* sequence could be facilitated with TraFo particles instead of using RNPs or AAV vectors with limited packaging capacity and can be combined with techniques that allow for the expression of sgRNAs and the delivery of HDR templates from AAV vectors.[69,70] In the context of other nucleases (zinc finger, TALE nuclease, and megaTALS), such co-delivery of AAV vectors with synthetic mRNAs has been previously reported.[71–75] In this context, TraFo-Cas9 delivery could be considered as an interesting option as it possesses all positive characteristics of transient Cas9 expression, while maintaining the high transductional efficiency and scalability of retroviral vectors. Because our system relies on no structural changes to the encapsidated nucleic acid or the thereof translated protein, the TraFo system can be useful wherever short protein availability is required. Particularly in view of newly emerging Cas9 variants and other promising members of the CRISPR family, such adaptability for transient transduction could be of value.

In summary, we could show that the TraFo-CRISPR/Cas9 vector system represents an efficient gene inactivation tool in U2OS, HeLa and Jurkat cells as well as primary MEF and human T cells. At the same time, the TraFo-Cas9 system provides significantly higher target specificity, than Cas9 delivery and expression by ICLVs or IDLVs. In addition, we demonstrate, that the Trafo-CRISPR/Cas9 vector system can also be used for HDR-mediated sequence-specific knock in by including a respective repair matrix in the sgRNA vector component. Finally, the ability to add negative selection marker expression cassettes (e.g., fluorescent proteins) may simplify discrimination, quantification, and isolation of cells with correct editing events from those having unintended additional genetic modifications.

MATERIAL AND METHODS

Cells and Culture Conditions

The HEK cell line 293T (ATCC CRL-1573),[76] the human epithelium HeLa cell line (ATCC CCL-2),[77] and the human osteosarcoma U-2 OS cell line (ATCC HTB-96), as well as a variant thereof U2OS-GFP[37,38] (a gift from Tony Cathomen) harboring a single lentiviral vector genome integrant with a constitutively expressed, CMV promoter-driven destabilized EGFP-PEST (dsEGFP) reporter protein ORF, were cultivated in DMEM supplemented with 10% heat-inactivated fetal calf serum and antibiotics. Bulk populations of U2OS-GFP cells stably expressing *egfp*-specific sgRNAs (U2OS-GFP sgEGFP1, sgEGFPwt) were generated by transduction of parental cells with IDPVs containing the respective U6 promoter driven sgRNA expression cassette. Primary mouse embryonic fibroblast cultures (MEF-GFP) were isolated from E12.5 embryos of CByJ.B6-Tg(UBC-GFP) 30Scha/J mice[78,79] and cultured in DMEM (+GlutaMaX, 10% FCS, 100 U/mL Penicillin, 100 µg/mL Streptomycin, 1× non-essential amino acids, 100 µM β-mercaptoethanol). The human T lymphocyte Jurkat cell line (ATCC TIB-152) was cultivated in RPMI supplemented with 10% heat-inactivated fetal calf serum, 1% non-essential amino acids, 1% sodium pyruvate, and 1% L-alanine, L-glutamate.

Recombinant Plasmid DNAs

Recombinant PFV vector particles were generated with a four-component vector system, which has been described previously.[32,80,81] Briefly, it consists of the expression-optimized packaging constructs pcoPG4 (PFV Gag), pcoPE (PFV Env), or pcoSE (SFVmcy Env), pcoPP (Pol), and different variants of the PFV transfer vector puc2MD9, as indicated. In some experiments, a previously described variant of the PFV Pol packaging construct, containing an ORF with catalytically inactive integrase (pcoPP3, Pol iIN, $D_{936}A$ mutation), was used.[80,82] In addition, we made use of a recently described three-component PFV RNA transfer vector system (TraFo) for transient genetic modification of target tissue by transfer of

non-viral RNAs.[35] For production of TraFo particles pseudotyped with VSV-G, an expression-optimized version of a PFV Gag packaging plasmid (pcoPG4 M6), encoding a PFV Gag protein with an N-terminal an HIV-1 Gag matrix domain enabling PFV Env independent particle egress,[83] and pcziVSV-G were used.[33] A schematic outline of the packaging components is shown in Figures S1C and S1D. *SpCas9* ORFs used in this study were derived from JDS246 (a gift from Keith Joung, Addgene plasmid #43861) or pL-CRISPR.ESF.tRFP (a gift from Benjamin Ebert, Addgene plasmid #57819[84]). U6 promoter-driven sgRNA expression cassettes were derived from pFYF1320 EGFP site #1 (a gift from Keith Joung, Addgene plasmid #47511[85]). The *iRFP670* ORF used in this study was derived from piRFP670-N1 (a gift from Vladislav Verkhusha, Addgene plasmid #45457[86]). Targeting sequences of the sgRNAs used in this study are listed in Table S1. Schematic outlines of the expression constructs encoding the different *Cas9* and/or *sgRNA*-encoding vector genomes are shown in Figure 3A, 5A and 5D, 7A, S1C, S1D, S5A, and S5B. All newly generated expression constructs were verified by diagnostic digest and sequencing analysis. Primer sequences and additional details are available upon request.

Lentiviral particles pseudotyped with PFV Env were produced using the mutant PFV Env packaging vector pcoPE01, the HIV-1 Gag-Pol-expressing packaging vector pCD/NL-BH and HIV-1 transfer vectors based on p6NST60[35,87,88] or pL-CRISPR.EFS.tRFP (a gift from Benjamin Ebert, Addgene plasmid #57819[84]). An HIV-1 packaging construct variant for production of IDLVs, pCD/NL-BH ΔIN, was generated by introducing a D64V mutation in the active center of the integrase domain in the *Pol* ORF of pCD/NL-BH.

Viral Vector Production and Target Cell Transduction

Cell culture supernatants containing recombinant viral particles were generated by transfection of the corresponding plasmids into 293T cells using polyethyleneimine (PEI) as described previously.[35,80,82] Plain, cell-free (0.45 μm filtered) viral supernatants in complete RPMI 1640 (for Jurkat and primary human T cells) or DMEM (all other cells) were used, either freshly harvested or stored frozen at −80°C. For transduction of primary human T cells, cell-free virus supernatants were concentrated 100-fold (v/v) by ultracentrifugation (SW32 Ti Rotor, 25,000 rpm, 90 min, 4°C) and the virus pellet was gently resuspended in complete RPMI 1640 medium and stored in aliquots at −80°C.

TraFo, ICRV, and IDRV supernatants were titrated in serial dilutions on U2OS-GFP cells or variants thereof stably expressing *egfp*-specific sgRNA (U2OS-GFP sgEGFP1, sgEGFPwt). In the case of *Cas9*-encoding TraFo, ICRV, and IDRV, the percentage of U2OS-GFP sgEGFP1/wt cells not expressing GFP was determined by flow cytometry 3 days or 8 days p.i. Furthermore, for ICRV and IDRV encoding in addition to *Cas9* or *sgRNA* a fluorescent reporter (*DsRed* or *iRFP*), the percentage of vector encoded fluorescent marker expressing cells was determined by flow cytometry at 2 or 3 days p.i. (depicted in individual figure legend). Viral titers were then calculated from the percentage of fluorescent reporter negative or positive cells as described previously.[33] MOIs calculated from fluorescent reporter coexpression are labeled as MOI-FR, whereas MOIs based on gene KO are labeled as MOI-KO.

HeLa Kyoto and U2OS-GFP target cells were seeded at a density of 2.5×10^4 cells/mL in 12-well plates 16–24 h prior to transduction. For transduction, target cells were incubated with 1 mL viral vector supernatants for 4–5 h. Combined virus infections were conducted simultaneously at 1:1 volume ratio of plain viral vector supernatants if not stated otherwise. Following aspiration of vector supernatants, transduced target cells were cultivated in fresh growth medium for different time periods as indicated.

For transduction of Jurkat cells, 2×10^5 cells in 10 μL volume were added to 500 μL of ICLV/IDLV sgRNA-TraFo-Cas9 (1:4 ratio) supernatant in complete RPMI 1640 medium in 48-well plates. Cell-virus mixtures were spinoculated (600 g, 2 h, 36°C) and subsequently cultivated overnight at 37%, 5% CO_2. On the next day, cells were pelleted and resuspended in fresh RPMI medium. Cells were cultured at a density of approximately 5×10^5 cells/mL every other day until the day of analysis. Primary human T cells were isolated from buffy coats obtained from healthy donors (DRK, German Red Cross, Dresden, Germany) using CD4 and CD8 coated magnetic bead sorting (Miltenyi, Bergisch-Gladbach, Germany). Isolated T cells were taken into culture in cytokine-supplemented medium (TexMACS, Miltenyi, Bergisch-Gladbach, Germany), activated using TransAct reagent (Miltenyi) as recommended by the manufacturer and transduced in the same way as described for Jurkat cells. Pan TCR α/β cell surface staining analyzed by flow cytometry on day 7 p.i. was used as the readout for successful gene engineering.

Gene Inactivation and Editing Analysis

For all viral transductions of CRISPR/Cas9 components into U2OS-GFP target cells, the percentage of non-fluorescence or changed-fluorescent color indicating gene inactivation or editing, respectively, was analyzed by flow cytometry at various time points post-transduction as indicated. Flow cytometry analysis was conducted on a FACSCalibur (Becton Dickinson) or MACSQuant analyzer (Miltenyi Biotec). All transduction experiments were performed at least three times using virus supernatants derived from independent transfections if not stated otherwise. The efficiency of *egfp* ORF inactivation in U2OS-GFP cells was calculated by the percentage of non-fluorescent cells at the given time point. Gene editing was determined by the fluorescent change from GFP to either DsRed or BFP.[50] Additional fluorescent reporter proteins (e.g., iRFP670) were used to determine residual or additional viral genome integrations into host cell chromatin of U2OS-GFP target cell populations with inactivated (GFP^-) or edited ($DsRed^+$ or BFP^+) *egfp* ORF. For T cell receptor KO analysis, 1×10^5 Jurkat cells or primary T cells were once washed with AutoMACS Running Buffer (AMRB) (Miltenyi Biotec, Bergisch Gladbach, Germany) and resuspended in 50 μL of PAN α/β staining solution (1:100) (mouse IP26A; IgG1 isotype; Beckman coulter). Cells were kept on ice for 45 min without light and washed 3× with AMRB. Subsequently, cells were diluted 1:40 with DAPI solution (1 mg/mL) and examined by flow cytometric analysis.

Off-Target Analysis

U2OS-GFP cells were seeded in 6-well plates at a density of 4.5×10^4 cells in 3 mL (1.5×10^4 cell/mL). On the next day, cells were incubated for 4–5 h with undiluted PFV particle supernatant transducing corresponding *egfp*-specific sgRNA expression cassettes (sgEGFPwt, m1, m2). 3 days after infection, cells were reseeded with a density of 2.5×10^4 cells/mL in 12-well plates and examined for their DsRed expression with fluorescence activated cell sorting (FACS) in order to evaluate the sgRNA transduction efficiency. Individual target cell populations with *egfp*-specific sgRNAs (wt, m1, m2) were infected 1 day later with 1:30 dilutions of ICLV, IDLV, or TraFo-Cas9 vector supernatant transducing the genetic information for Cas9. Cells were incubated for 4–5 h with the appropriate virus supernatants and analyzed for their GFP and DsRed fluorescence with FACS 3 and 8 days later. Targeting specificity of different Cas9 transductions was calculated using the GFP inactivation efficiency with perfectly matching sgRNA as a multiple of inactivation efficiency with mismatch sgRNA m1 or m2.[21]

Western Blot Analysis

HeLa cells co-transduced with TraFo-Cas9 vector and sgRNA-HDR vector supernatants as indicated were selected with Puromycin (2 μg/mL) for 11 days, treated with Nocodazole (0.1 μg/mL) for 12 h, and enriched by flow cytometry sorting according to their GFP and DsRed fluorescence intensity. Parental, puromycin-resistant cell populations, as well as enriched cell populations, were grown on a 100-mm cell culture dish, treated overnight with Nocodazole (0.1 μg/mL), and lysed in detergent-containing buffer. Cell lysates were subsequently centrifuged through a QIAshredder column (QIAGEN). Aliquots of cell extracts were separated by SDS-PAGE on self-made 10% polyacrylamide or a Bis-Tris precast gels (NuPAGE) and analyzed by immunoblotting using specific antibodies as described previously.[89] Antibodies used were a mixture of two monoclonal mouse antibodies specific for GFP (7.1, 13.1; Roche 11814460001), a mouse monoclonal antibody recognizing amino acid (aa) 261–412 in the internal region of PLK1 (F-8; sc-17783, Santa Cruz, CA, USA), a GAPDH-specific rabbit monoclonal antibody (G9545; Sigma), or an mCherry-specific rabbit polyclonal antiserum (399C[90]). For chemiluminescence detection, appropriate horseradish peroxidase (HRP)-conjugated secondary antibodies were used, and blots were developed with Immobilon Western HRP substrate. Chemiluminescent signals were digitally recorded using a LAS-3000 (Fujifilm) imager and quantified using ImageGauge (Fujifilm).

Confocal Microscopy

The spatiotemporal distribution of N-terminal GFP-tagged, endogenous PLK was analyzed using confocal microscopy and executed as described previously.[80] Puromycin selected (2 μg/mL) and sorted cells were replated at a concentration of 3×10^4 cells per well on poly-L-lysine coated coverslips in 12-well plates. At 48 h post-seeding, the cells were washed with cold PBS, fixed with 3% paraformaldehyde, and the cell nuclei were stained with DAPI for 5 min. Finally, the cells were covered with Mowiol. Confocal laser scanning images were obtained on a Zeiss LSM 510 using a Zeiss Apochromat 63×, NA 1.4 oil immersion objective. Fluorescence images were evaluated using ImageJ software

Live Cell Imaging

16–24 h prior to transduction, 2×10^4 cells/mL U2OS-GFP cells were seeded in a 12-well plate. Cells were incubated for 4–5 h at 37°C, 5% CO_2 with TraFo-Cas9 and IDPV sgRNA-HDR vector supernatants simultaneously at a 1:1 volume ratio. Virus transduction was stopped by exchange with fresh medium. 1 day later, cells were transferred to a cell culture incubator equipped with an IncuCyte Zoom Live Cell Imaging System (Essen BioScience) and GFP and DsRed fluorescence monitored at 1 h intervals for 80 h.

qPCR Analysis

Preparation of cellular samples for qPCR analysis was performed as previously described.[35,80] Primers, Taqman probes, and cycling conditions for specific quantification of Cas9, sequence integration, or human β-actin are summarized in Table S2.

Statistical Analysis

If not stated otherwise, data are shown as means ± SD. Bar charts are shown with scatterplots of individual data points. Statistical analysis was performed using Welch's t test (unpaired t test, two-tailed, 95% confidence intervals). Significance levels in each figure are indicated by asterisks ($^*p \leq 0.05$, $^{**}p < 0.01$, $^{***}p < 0.005$).

SUPPLEMENTAL INFORMATION

Supplemental Information can be found online at https://doi.org/10.1016/j.omtn.2019.10.006.

AUTHOR CONTRIBUTIONS

Performed the experiments: F.L., C.R.D., J.D., N.W., M.N., F.B., S.F., and M.V.H. Analyzed the data: F.L., C.R.D., J.D., N.W., M.N., F.B., and M.V.H. Contributed reagents/materials/analysis tools: R.B. Wrote the paper: F.L., N.W., R.B., M.C., M.V.H., and D.L. All authors read and approved the final manuscript.

CONFLICTS OF INTEREST

The authors declare no competing interests.

ACKNOWLEDGMENTS

This work was supported by a seed grant of the DFG-Center for Regenerative Therapies Dresden (CRTD, FZT111) to D.L. We acknowledge support by the Open Access Publication Funds of the SLUB/TU Dresden.

REFERENCES

1. Jinek, M., East, A., Cheng, A., Lin, S., Ma, E., and Doudna, J. (2013). RNA-programmed genome editing in human cells. eLife *2*, e00471.

2. Mali, P., Yang, L., Esvelt, K.M., Aach, J., Guell, M., DiCarlo, J.E., Norville, J.E., and Church, G.M. (2013). RNA-guided human genome engineering via Cas9. Science *339*, 823–826.

3. Cong, L., Ran, F.A., Cox, D., Lin, S., Barretto, R., Habib, N., Hsu, P.D., Wu, X., Jiang, W., Marraffini, L.A., and Zhang, F. (2013). Multiplex genome engineering using CRISPR/Cas systems. Science *339*, 819–823.

4. Nelson, C.E., Hakim, C.H., Ousterout, D.G., Thakore, P.I., Moreb, E.A., Castellanos Rivera, R.M., Madhavan, S., Pan, X., Ran, F.A., Yan, W.X., et al. (2016). In vivo genome editing improves muscle function in a mouse model of Duchenne muscular dystrophy. Science *351*, 403–407.

5. Doudna, J.A., and Charpentier, E. (2014). Genome editing. The new frontier of genome engineering with CRISPR-Cas9. Science *346*, 1258096.

6. Ran, F.A., Cong, L., Yan, W.X., Scott, D.A., Gootenberg, J.S., Kriz, A.J., Zetsche, B., Shalem, O., Wu, X., Makarova, K.S., et al. (2015). In vivo genome editing using Staphylococcus aureus Cas9. Nature *520*, 186–191.

7. Cox, D.B., Platt, R.J., and Zhang, F. (2015). Therapeutic genome editing: prospects and challenges. Nat. Med. *21*, 121–131.

8. Kleinstiver, B.P., Pattanayak, V., Prew, M.S., Tsai, S.Q., Nguyen, N.T., Zheng, Z., and Joung, J.K. (2016). High-fidelity CRISPR-Cas9 nucleases with no detectable genome-wide off-target effects. Nature *529*, 490–495.

9. Slaymaker, I.M., Gao, L., Zetsche, B., Scott, D.A., Yan, W.X., and Zhang, F. (2016). Rationally engineered Cas9 nucleases with improved specificity. Science *351*, 84–88.

10. Shalem, O., Sanjana, N.E., Hartenian, E., Shi, X., Scott, D.A., Mikkelson, T., Heckl, D., Ebert, B.L., Root, D.E., Doench, J.G., and Zhang, F. (2014). Genome-scale CRISPR-Cas9 knockout screening in human cells. Science *343*, 84–87.

11. Kim, S., Kim, D., Cho, S.W., Kim, J., and Kim, J.S. (2014). Highly efficient RNA-guided genome editing in human cells via delivery of purified Cas9 ribonucleoproteins. Genome Res. *24*, 1012–1019.

12. Pattanayak, V., Lin, S., Guilinger, J.P., Ma, E., Doudna, J.A., and Liu, D.R. (2013). High-throughput profiling of off-target DNA cleavage reveals RNA-programmed Cas9 nuclease specificity. Nat. Biotechnol. *31*, 839–843.

13. Fu, B.X., Hansen, L.L., Artiles, K.L., Nonet, M.L., and Fire, A.Z. (2014). Landscape of target:guide homology effects on Cas9-mediated cleavage. Nucleic Acids Res. *42*, 13778–13787.

14. Hsu, P.D., Scott, D.A., Weinstein, J.A., Ran, F.A., Konermann, S., Agarwala, V., Li, Y., Fine, E.J., Wu, X., Shalem, O., et al. (2013). DNA targeting specificity of RNA-guided Cas9 nucleases. Nat. Biotechnol. *31*, 827–832.

15. Liang, X., Potter, J., Kumar, S., Zou, Y., Quintanilla, R., Sridharan, M., Carte, J., Chen, W., Roark, N., Ranganathan, S., et al. (2015). Rapid and highly efficient mammalian cell engineering via Cas9 protein transfection. J. Biotechnol. *208*, 44–53.

16. Yin, H., Song, C.Q., Dorkin, J.R., Zhu, L.J., Li, Y., Wu, Q., Park, A., Yang, J., Suresh, S., Bizhanova, A., et al. (2016). Therapeutic genome editing by combined viral and non-viral delivery of CRISPR system components in vivo. Nat. Biotechnol. *34*, 328–333.

17. Holkers, M., Maggio, I., Henriques, S.F., Janssen, J.M., Cathomen, T., and Gonçalves, M.A. (2014). Adenoviral vector DNA for accurate genome editing with engineered nucleases. Nat. Methods *11*, 1051–1057.

18. Kabadi, A.M., Ousterout, D.G., Hilton, I.B., and Gersbach, C.A. (2014). Multiplex CRISPR/Cas9-based genome engineering from a single lentiviral vector. Nucleic Acids Res. *42*, e147.

19. Nelson, C.E., and Gersbach, C.A. (2016). Engineering Delivery Vehicles for Genome Editing. Annu. Rev. Chem. Biomol. Eng. *7*, 637–662.

20. Ortinski, P.I., O'Donovan, B., Dong, X., and Kantor, B. (2017). Integrase-Deficient Lentiviral Vector as an All-in-One Platform for Highly Efficient CRISPR/Cas9-Mediated Gene Editing. Mol. Ther. Methods Clin. Dev. *5*, 153–164.

21. Petris, G., Casini, A., Montagna, C., Lorenzin, F., Prandi, D., Romanel, A., Zasso, J., Conti, L., Demichelis, F., and Cereseto, A. (2017). Hit and go CAS9 delivered through a lentiviral based self-limiting circuit. Nat. Commun. *8*, 15334.

22. Merienne, N., Vachey, G., de Longprez, L., Meunier, C., Zimmer, V., Perriard, G., Canales, M., Mathias, A., Herrgott, L., Beltraminelli, T., et al. (2017). The Self-Inactivating KamiCas9 System for the Editing of CNS Disease Genes. Cell Rep. *20*, 2980–2991.

23. Choi, J.G., Dang, Y., Abraham, S., Ma, H., Zhang, J., Guo, H., Cai, Y., Mikkelsen, J.G., Wu, H., Shankar, P., and Manjunath, N. (2016). Lentivirus pre-packed with Cas9 protein for safer gene editing. Gene Ther. *23*, 627–633.

24. Rethwilm, A., and Lindemann, D. (2013). Foamy Viruses. In Fields Virology, Sixth Edition, *Volume 2*, D.M. Knipe and P.M. Howley, eds (Lippincott Williams & Wilkins), pp. 1613–1632.

25. Lindemann, D., and Rethwilm, A. (2011). Foamy virus biology and its application for vector development. Viruses *3*, 561–585.

26. Trobridge, G.D., Horn, P.A., Beard, B.C., and Kiem, H.P. (2012). Large animal models for foamy virus vector gene therapy. Viruses *4*, 3572–3588.

27. Sweeney, N.P., Regan, C., Liu, J., Galleu, A., Dazzi, F., Lindemann, D., Rupar, C.A., and McClure, M.O. (2016). Rapid and Efficient Stable Gene Transfer to Mesenchymal Stromal Cells Using a Modified Foamy Virus Vector. Mol. Ther. *24*, 1227–1236.

28. Bauer, T.R., Jr., Tuschong, L.M., Calvo, K.R., Shive, H.R., Burkholder, T.H., Karlsson, E.K., West, R.R., Russell, D.W., and Hickstein, D.D. (2013). Long-term follow-up of foamy viral vector-mediated gene therapy for canine leukocyte adhesion deficiency. Mol. Ther. *21*, 964–972.

29. Bauer, T.R., Jr., Allen, J.M., Hai, M., Tuschong, L.M., Khan, I.F., Olson, E.M., Adler, R.L., Burkholder, T.H., Gu, Y.C., Russell, D.W., and Hickstein, D.D. (2008). Successful treatment of canine leukocyte adhesion deficiency by foamy virus vectors. Nat. Med. *14*, 93–97.

30. Burtner, C.R., Beard, B.C., Kennedy, D.R., Wohlfahrt, M.E., Adair, J.E., Trobridge, G.D., Scharenberg, A.M., Torgerson, T.R., Rawlings, D.J., Felsburg, P.J., and Kiem, H.P. (2014). Intravenous injection of a foamy virus vector to correct canine SCID-X1. Blood *123*, 3578–3584.

31. Vassilopoulos, G., Trobridge, G., Josephson, N.C., and Russell, D.W. (2001). Gene transfer into murine hematopoietic stem cells with helper-free foamy virus vectors. Blood *98*, 604–609.

32. Heinkelein, M., Dressler, M., Jármy, G., Rammling, M., Imrich, H., Thurow, J., Lindemann, D., and Rethwilm, A. (2002). Improved primate foamy virus vectors and packaging constructs. J. Virol. *76*, 3774–3783.

33. Ho, Y.P., Schnabel, V., Swiersy, A., Stirnnagel, K., and Lindemann, D. (2012). A small-molecule-controlled system for efficient pseudotyping of prototype foamy virus vectors. Mol. Ther. *20*, 1167–1176.

34. Deyle, D.R., Li, Y., Olson, E.M., and Russell, D.W. (2010). Nonintegrating foamy virus vectors. J. Virol. *84*, 9341–9349.

35. Hamann, M.V., Stanke, N., Müllers, E., Stirnnagel, K., Hütter, S., Artegiani, B., Bragado Alonso, S., Calegari, F., and Lindemann, D. (2014). Efficient transient genetic manipulation in vitro and in vivo by prototype foamy virus-mediated nonviral RNA transfer. Mol. Ther. *22*, 1460–1471.

36. Hamann, M.V., Müllers, E., Reh, J., Stanke, N., Effantin, G., Weissenhorn, W., and Lindemann, D. (2014). The cooperative function of arginine residues in the Prototype Foamy Virus Gag C-terminus mediates viral and cellular RNA encapsidation. Retrovirology *11*, 87.

37. Reyon, D., Tsai, S.Q., Khayter, C., Foden, J.A., Sander, J.D., and Joung, J.K. (2012). FLASH assembly of TALENs for high-throughput genome editing. Nat. Biotechnol. *30*, 460–465.

38. Händel, E.M., Gellhaus, K., Khan, K., Bednarski, C., Cornu, T.I., Müller-Lerch, F., Kotin, R.M., Heilbronn, R., and Cathomen, T. (2012). Versatile and efficient genome editing in human cells by combining zinc-finger nucleases with adeno-associated viral vectors. Hum. Gene Ther. *23*, 321–329.

39. Mátrai, J., Cantore, A., Bartholomae, C.C., Annoni, A., Wang, W., Acosta-Sanchez, A., Samara-Kuko, E., De Waele, L., Ma, L., Genovese, P., et al. (2011). Hepatocyte-targeted expression by integrase-defective lentiviral vectors induces antigen-specific tolerance in mice with low genotoxic risk. Hepatology *53*, 1696–1707.

40. Nightingale, S.J., Hollis, R.P., Pepper, K.A., Petersen, D., Yu, X.J., Yang, C., Bahner, I., and Kohn, D.B. (2006). Transient gene expression by nonintegrating lentiviral vectors. Mol. Ther. *13*, 1121–1132.

41. Merrihew, R.V., Marburger, K., Pennington, S.L., Roth, D.B., and Wilson, J.H. (1996). High-frequency illegitimate integration of transfected DNA at preintegrated target sites in a mammalian genome. Mol. Cell. Biol. *16*, 10–18.

42. Murnane, J.P., Yezzi, M.J., and Young, B.R. (1990). Recombination events during integration of transfected DNA into normal human cells. Nucleic Acids Res. *18*, 2733–2738.

43. Daniyan, A.F., and Brentjens, R.J. (2019). CARs of the future. Am. J. Hematol. *94* (S1), S55–S58.

44. Boyiadzis, M.M., Dhodapkar, M.V., Brentjens, R.J., Kochenderfer, J.N., Neelapu, S.S., Maus, M.V., Porter, D.L., Maloney, D.G., Grupp, S.A., Mackall, C.L., et al. (2018). Chimeric antigen receptor (CAR) T therapies for the treatment of hematologic malignancies: clinical perspective and significance. J. Immunother. Cancer *6*, 137.

45. Rivière, I., and Sadelain, M. (2017). Chimeric Antigen Receptors: A Cell and Gene Therapy Perspective. Mol. Ther. *25*, 1117–1124.

46. Ren, J., Zhang, X., Liu, X., Fang, C., Jiang, S., June, C.H., and Zhao, Y. (2017). A versatile system for rapid multiplex genome-edited CAR T cell generation. Oncotarget *8*, 17002–17011.

47. Vatakis, D.N., Kim, S., Kim, N., Chow, S.A., and Zack, J.A. (2009). Human immunodeficiency virus integration efficiency and site selection in quiescent CD4+ T cells. J. Virol. *83*, 6222–6233.

48. Donahue, D.A., Sloan, R.D., Kuhl, B.D., Bar-Magen, T., Schader, S.M., and Wainberg, M.A. (2010). Stage-dependent inhibition of HIV-1 replication by antiretroviral drugs in cell culture. Antimicrob. Agents Chemother. *54*, 1047–1054.

49. Uchida, N., Green, R., Ballantine, J., Skala, L.P., Hsieh, M.M., and Tisdale, J.F. (2016). Kinetics of lentiviral vector transduction in human CD34(+) cells. Exp. Hematol. *44*, 106–115.

50. Glaser, A., McColl, B., and Vadolas, J. (2016). GFP to BFP Conversion: A Versatile Assay for the Quantification of CRISPR/Cas9-mediated Genome Editing. Mol. Ther. Nucleic Acids *5*, e334.

51. Archambault, V., Lépine, G., and Kachaner, D. (2015). Understanding the Polo Kinase machine. Oncogene *34*, 4799–4807.

52. Archambault, V., and Glover, D.M. (2009). Polo-like kinases: conservation and divergence in their functions and regulation. Nat. Rev. Mol. Cell Biol. *10*, 265–275.

53. Wang, D., Mou, H., Li, S., Li, Y., Hough, S., Tran, K., Li, J., Yin, H., Anderson, D.G., Sontheimer, E.J., et al. (2015). Adenovirus-Mediated Somatic Genome Editing of Pten by CRISPR/Cas9 in Mouse Liver in Spite of Cas9-Specific Immune Responses. Hum. Gene Ther. *26*, 432–442.

54. Chew, W.L. (2018). Immunity to CRISPR Cas9 and Cas12a therapeutics. Wiley Interdiscip. Rev. Syst. Biol. Med. *10*, e1408.

55. Wang, X., Wang, Y., Wu, X., Wang, J., Wang, Y., Qiu, Z., Chang, T., Huang, H., Lin, R.J., and Yee, J.K. (2015). Unbiased detection of off-target cleavage by CRISPR-Cas9 and TALENs using integrase-defective lentiviral vectors. Nat. Biotechnol. *33*, 175–178.

56. Gabriel, R., Lombardo, A., Arens, A., Miller, J.C., Genovese, P., Kaeppel, C., Nowrouzi, A., Bartholomae, C.C., Wang, J., Friedman, G., et al. (2011). An unbiased genome-wide analysis of zinc-finger nuclease specificity. Nat. Biotechnol. *29*, 816–823.

57. Wang, Y., Wang, Y., Chang, T., Huang, H., and Yee, J.K. (2017). Integration-defective lentiviral vector mediates efficient gene editing through homology-directed repair in human embryonic stem cells. Nucleic Acids Res. *45*, e29.

58. Lee, J.S., Kallehauge, T.B., Pedersen, L.E., and Kildegaard, H.F. (2015). Site-specific integration in CHO cells mediated by CRISPR/Cas9 and homology-directed DNA repair pathway. Sci. Rep. *5*, 8572.

59. Zuris, J.A., Thompson, D.B., Shu, Y., Guilinger, J.P., Bessen, J.L., Hu, J.H., Maeder, M.L., Joung, J.K., Chen, Z.Y., and Liu, D.R. (2015). Cationic lipid-mediated delivery of proteins enables efficient protein-based genome editing in vitro and in vivo. Nat. Biotechnol. *33*, 73–80.

60. Eyquem, J., Mansilla-Soto, J., Giavridis, T., van der Stegen, S.J., Hamieh, M., Cunanan, K.M., Odak, A., Gönen, M., and Sadelain, M. (2017). Targeting a CAR to the TRAC locus with CRISPR/Cas9 enhances tumour rejection. Nature *543*, 113–117.

61. Köhler, A., and Hurt, E. (2007). Exporting RNA from the nucleus to the cytoplasm. Nat. Rev. Mol. Cell Biol. *8*, 761–773.

62. Montagna, C., Petris, G., Casini, A., Maule, G., Franceschini, G.M., Zanella, I., Conti, L., Arnoldi, F., Burrone, O.R., Zentilin, L., et al. (2018). VSV-G-Enveloped Vesicles for Traceless Delivery of CRISPR-Cas9. Mol. Ther. Nucleic Acids *12*, 453–462.

63. Ramakrishna, S., Kwaku Dad, A.B., Beloor, J., Gopalappa, R., Lee, S.K., and Kim, H. (2014). Gene disruption by cell-penetrating peptide-mediated delivery of Cas9 protein and guide RNA. Genome Res. *24*, 1020–1027.

64. Knopp, Y., Geis, F.K., Heckl, D., Horn, S., Neumann, T., Kuehle, J., Meyer, J., Fehse, B., Baum, C., Morgan, M., et al. (2018). Transient Retrovirus-Based CRISPR/Cas9 All-in-One Particles for Efficient, Targeted Gene Knockout. Mol. Ther. Nucleic Acids *13*, 256–274.

65. Lu, B., Javidi-Parsijani, P., Makani, V., Mehraein-Ghomi, F., Sarhan, W.M., Sun, D., Yoo, K.W., Atala, Z.P., Lyu, P., and Atala, A. (2019). Delivering SaCas9 mRNA by lentivirus-like bionanoparticles for transient expression and efficient genome editing. Nucleic Acids Res. *47*, e44.

66. Lyu, P., Javidi-Parsijani, P., Atala, A., and Lu, B. (2019). Delivering Cas9/sgRNA ribonucleoprotein (RNP) by lentiviral capsid-based bionanoparticles for efficient 'hit-and-run' genome editing. Nucleic Acids Res. *47*, e99.

67. Miller, D.G., Petek, L.M., and Russell, D.W. (2004). Adeno-associated virus vectors integrate at chromosome breakage sites. Nat. Genet. *36*, 767–773.

68. Gaj, T., Staahl, B.T., Rodrigues, G.M.C., Limsirichai, P., Ekman, F.K., Doudna, J.A., and Schaffer, D.V. (2017). Targeted gene knock-in by homology-directed genome editing using Cas9 ribonucleoprotein and AAV donor delivery. Nucleic Acids Res. *45*, e98.

69. Matharu, N., Rattanasopha, S., Tamura, S., Maliskova, L., Wang, Y., Bernard, A., Hardin, A., Eckalbar, W.L., Vaisse, C., and Ahituv, N. (2019). CRISPR-mediated activation of a promoter or enhancer rescues obesity caused by haploinsufficiency. Science *363*, eaau0629.

70. Ohmori, T., Nagao, Y., Mizukami, H., Sakata, A., Muramatsu, S.I., Ozawa, K., Tominaga, S.I., Hanazono, Y., Nishimura, S., Nureki, O., and Sakata, Y. (2017). CRISPR/Cas9-mediated genome editing via postnatal administration of AAV vector cures haemophilia B mice. Sci. Rep. *7*, 4159.

71. Wang, J., Exline, C.M., DeClercq, J.J., Llewellyn, G.N., Hayward, S.B., Li, P.W., Shivak, D.A., Surosky, R.T., Gregory, P.D., Holmes, M.C., and Cannon, P.M. (2015). Homology-driven genome editing in hematopoietic stem and progenitor cells using ZFN mRNA and AAV6 donors. Nat. Biotechnol. *33*, 1256–1263.

72. Wang, J., DeClercq, J.J., Hayward, S.B., Li, P.W., Shivak, D.A., Gregory, P.D., Lee, G., and Holmes, M.C. (2016). Highly efficient homology-driven genome editing in human T cells by combining zinc-finger nuclease mRNA and AAV6 donor delivery. Nucleic Acids Res. *44*, e30.

73. De Ravin, S.S., Reik, A., Liu, P.Q., Li, L., Wu, X., Su, L., Raley, C., Theobald, N., Choi, U., Song, A.H., et al. (2016). Targeted gene addition in human CD34(+) hematopoietic cells for correction of X-linked chronic granulomatous disease. Nat. Biotechnol. *34*, 424–429.

74. Mahiny, A.J., Dewerth, A., Mays, L.E., Alkhaled, M., Mothes, B., Malaeksefat, E., Loretz, B., Rottenberger, J., Brosch, D.M., Reautschnig, P., et al. (2015). In vivo genome editing using nuclease-encoding mRNA corrects SP-B deficiency. Nat. Biotechnol. *33*, 584–586.

75. Sather, B.D., Romano Ibarra, G.S., Sommer, K., Curinga, G., Hale, M., Khan, I.F., Singh, S., Song, Y., Gwiazda, K., Sahni, J., et al. (2015). Efficient modification of CCR5 in primary human hematopoietic cells using a megaTAL nuclease and AAV donor template. Sci. Transl. Med. *7*, 307ra156.

76. DuBridge, R.B., Tang, P., Hsia, H.C., Leong, P.M., Miller, J.H., and Calos, M.P. (1987). Analysis of mutation in human cells by using an Epstein-Barr virus shuttle system. Mol. Cell. Biol. *7*, 379–387.

77. Shooter, R.A., and Gey, G.O. (1952). Studies of the mineral requirements of mammalian cells. Br. J. Exp. Pathol. *33*, 98–103.

78. Schaefer, B.C., Schaefer, M.L., Kappler, J.W., Marrack, P., and Kedl, R.M. (2001). Observation of antigen-dependent CD8+ T-cell/ dendritic cell interactions in vivo. Cell. Immunol. *214*, 110–122.

79. Joshi, M., Keith Pittman, H., Haisch, C., and Verbanac, K. (2008). Real-time PCR to determine transgene copy number and to quantitate the biolocalization of adoptively transferred cells from EGFP-transgenic mice. Biotechniques *45*, 247–258.

80. Müllers, E., Uhlig, T., Stirnnagel, K., Fiebig, U., Zentgraf, H., and Lindemann, D. (2011). Novel functions of prototype foamy virus Gag glycine- arginine-rich boxes in reverse transcription and particle morphogenesis. J. Virol. *85*, 1452–1463.

81. Stirnnagel, K., Lüftenegger, D., Stange, A., Swiersy, A., Müllers, E., Reh, J., Stanke, N., Grosse, A., Chiantia, S., Keller, H., et al. (2010). Analysis of prototype foamy virus particle-host cell interaction with autofluorescent retroviral particles. Retrovirology *7*, 45.

82. Hütter, S., Müllers, E., Stanke, N., Reh, J., and Lindemann, D. (2013). Prototype foamy virus protease activity is essential for intraparticle reverse transcription initiation but not absolutely required for uncoating upon host cell entry. J. Virol. *87*, 3163–3176.

83. Swiersy, A., Wiek, C., Zentgraf, H., and Lindemann, D. (2013). Characterization and manipulation of foamy virus membrane interactions. Cell. Microbiol. *15*, 227–236.

84. Heckl, D., Kowalczyk, M.S., Yudovich, D., Belizaire, R., Puram, R.V., McConkey, M.E., Thielke, A., Aster, J.C., Regev, A., and Ebert, B.L. (2014). Generation of mouse models of myeloid malignancy with combinatorial genetic lesions using CRISPR-Cas9 genome editing. Nat. Biotechnol. *32*, 941–946.

85. Fu, Y., Foden, J.A., Khayter, C., Maeder, M.L., Reyon, D., Joung, J.K., and Sander, J.D. (2013). High-frequency off-target mutagenesis induced by CRISPR-Cas nucleases in human cells. Nat. Biotechnol. *31*, 822–826.

86. Shcherbakova, D.M., and Verkhusha, V.V. (2013). Near-infrared fluorescent proteins for multicolor in vivo imaging. Nat. Methods *10*, 751–754.

87. Mochizuki, H., Schwartz, J.P., Tanaka, K., Brady, R.O., and Reiser, J. (1998). High-titer human immunodeficiency virus type 1-based vector systems for gene delivery into nondividing cells. J. Virol. *72*, 8873–8883.

88. Lindemann, D., Stirnnagel, K., and Lüftenegger, D. (2013). Foamy viral envelope genes. In Bulletin 2009/53, E.P. Office, ed., p. 55.

89. Zurnic, I., Hütter, S., Rzeha, U., Stanke, N., Reh, J., Müllers, E., Hamann, M.V., Kern, T., Gerresheim, G.K., Lindel, F., et al. (2016). Interactions of Prototype Foamy Virus Capsids with Host Cell Polo-Like Kinases Are Important for Efficient Viral DNA Integration. PLoS Pathog. *12*, e1005860.

90. Stirnnagel, K., Schupp, D., Dupont, A., Kudryavtsev, V., Reh, J., Müllers, E., Lamb, D.C., and Lindemann, D. (2012). Differential pH-dependent cellular uptake pathways among foamy viruses elucidated using dual-colored fluorescent particles. Retrovirology *9*, 71.